

RESEARCH

Open Access



Circular RNA circNRIP1 acts as a microRNA-149-5p sponge to promote gastric cancer progression via the AKT1/mTOR pathway

Xing Zhang^{1†}, Sen Wang^{1†}, Haixiao Wang^{4†}, Jiacheng Cao^{1†}, Xiaoxu Huang¹, Zheng Chen², Penghui Xu¹, Guangli Sun¹, Jianghao Xu¹, Jialun Lv¹ and Zekuan Xu^{1,3*} 

Abstract

Background: CircRNA has emerged as a new non-coding RNA that plays crucial roles in tumour initiation and development. 'MiRNA sponge' is the most reported role played by circRNAs in many tumours. The AKT/mTOR axis is a classic signalling pathway in cancers that sustains energy homeostasis through energy production activities, such as the Warburg effect, and blocks catabolic activities, such as autophagy. Additionally, the AKT/mTOR axis exerts a positive effect on EMT, which promotes tumour metastasis.

Methods: We detected higher circNRIP1 expression in gastric cancer by performing RNA-seq analysis. We verified the tumour promotor role of circNRIP1 in gastric cancer cells through a series of biological function assays. We then used a pull-down assay and dual-luciferase reporter assay to identify the downstream miR-149-5p of circNRIP1. Western blot analysis and immunofluorescence assays were performed to demonstrate that the circNRIP1-miR-149-5p-AKT1/mTOR axis is responsible for the altered metabolism in GC cells and promotes GC development. We then adopted a co-culture system to trace circNRIP1 transmission via exosomal communication and RIP experiments to determine that quaking regulates circNRIP1 expression. Finally, we confirmed the tumour suppressor role of microRNA-133a-3p in vivo in PDX mouse models.

Results: We discovered that knockdown of circNRIP1 successfully blocked proliferation, migration, invasion and the expression level of AKT1 in GC cells. MiR-149-5p inhibition phenocopied the overexpression of circNRIP1 in GC cells, and overexpression of miR-149-5p blocked the malignant behaviours of circNRIP1. Moreover, it was proven that circNRIP1 can be transmitted by exosomal communication between GC cells, and exosomal circNRIP1 promoted tumour metastasis in vivo. We also demonstrated that quaking can promote circNRIP1 transcription. In the final step, the tumour promotor role of circNRIP1 was verified in PDX models.

Conclusions: We proved that circNRIP1 sponges miR-149-5p to affect the expression level of AKT1 and eventually acts as a tumour promotor in GC.

Keywords: Gastric cancer, circRNA, miRNA, ceRNA, AKT1, Organoid, PDX model

* Correspondence: xuzekuan@njmu.edu.cn

[†]Xing Zhang, Sen Wang, Haixiao Wang and Jiacheng Cao contributed equally to this work.

¹Department of General Surgery, The First Affiliated Hospital of Nanjing Medical University, No.300, Guangzhou Road, Nanjing, Jiangsu Province, China

³Collaborative Innovation Center For Cancer Personalized Medicine, Nanjing Medical University, Nanjing 210029, Jiangsu Province, China

Full list of author information is available at the end of the article



Background

Gastric cancer (GC), also called stomach adenocarcinoma, has raised societal concerns worldwide, especially in East Asian countries in recent years. GC ranks as the fourth most frequent cancer and the third leading cause of cancer mortality worldwide according to the GLOBOCAN database [1–3]. Although many advancements have been achieved in terms of diagnostic methods and surgical procedures, the overall survival of GC patients has remained largely unsatisfactory in recent years. The 5-year overall survival is less than 30% in most countries [4]. The complexity of GC treatment lies in its heterogeneity within tumour tissues, not only due to genetic but also epigenetic alterations. Therefore, there is an urgent need to gain an in-depth understanding of the molecular mechanisms explaining GC initiation and development.

It has been reported that non-coding RNAs regulate the initiation and development of GC. MicroRNAs (miRNAs) and long non-coding RNAs (lncRNAs) are two major non-coding RNAs in tumour biology that have mainly been investigated due to their crucial roles [5–7]. CircRNA has emerged as a new non-coding RNA that is important in tumour initiation and development [8–10]. CircRNAs within eukaryotic cells were discovered 40 years ago. However, circRNAs are not properly understood and were identified as incorrect gene rearrangements and splicing errors until recently [11]. More functional circRNAs have been discovered thanks to high-throughput sequencing analysis and bioinformatic methods. CircRNAs are derived basically from the exons of their parental genes, although intronic and exonic-intronic circRNAs might sometimes occur [12, 13]. Exonic circRNAs are covalently connected and are structured in a head-to-tail closed loop [14]. This circular structure is responsible for its stable existence and abundance in GC tissues, which makes circular RNAs themselves hallmarks for the diagnosis and prognosis of GC. Moreover, circRNAs have been reported to have many important roles, including as protein sponges [15, 16], in translation [17, 18] and as miRNA sponges [19]. ‘miRNA sponge’ is the most commonly reported role of circRNAs in many tumours [20, 21]. Many RNA transcripts share binding sites with miRNAs, and they compete with one another to act as competing endogenous RNAs (ceRNAs) to further regulate tumour development [22, 23]. CircRNAs assume the role of ceRNAs by acting as miRNA sponges in many tumours [24]. For example, circHIPK3 sponges miR-558 to suppress heparanase expression in bladder cancer cells [25]; additionally, the circular RNA profile of circPVT1 identifies it as a proliferative factor and prognostic marker in gastric cancer, and circular RNA MTO1 acts as the sponge of miR-9 to suppress hepatocellular carcinoma progression [26].

However, some researchers still argue that not all miRNAs targeted by circRNAs are suppressed, and current ceRNA validation methods are limited [11].

It has been reported that mTOR acts as downstream molecule of AKT1, and the AKT/mTOR pathway is one of the classic signalling pathways to mediate tumour metabolic homeostasis, which is beneficial for tumour growth and metastasis [27]. The AKT/mTOR axis sustains energy homeostasis through energy production activities, such as the Warburg effect, to satisfy the proliferation needs of GC cells [28]. mTORC1 (mTOR complex consisting of mTORC1 and mTORC2) is reported to accelerate tumour growth by promoting a shift to the Warburg effect, which likely facilitates the incorporation of nutrients into new bio-products to sustain the highly proliferative character of GC cells. mTORC1 facilitates the expression level of the transcription factor HIF1 α , which increases the translation of several glycolytic enzymes, such as phospho-fructo kinase (PFK). Additionally, the AKT/mTOR axis enables anabolic metabolism, such as protein synthesis, and blocks catabolic activities, such as autophagy, to ultimately favour cell growth in GC [29, 30]. mTORC1 promotes cell growth by suppressing catabolic activities, including autophagy, to slow the aging of GC cells. mTORC1 phosphorylates ULK1 to prevent it from being activated by AMPK, a key activator of autophagy.

Autophagy inhibition is also of great importance for the well vascularized condition of GC tumours. Additionally, the AKT/mTOR axis is also reported to exert a positive role in EMT, promoting tumour metastasis.

Exosomes are reported to mediate the molecular communication and material transfer between primary tumour sites and distant metastasis sites [31, 32]. Exosomal communication maintains a very close relationship with tumour cell migration and invasion by regulating a series of cellular activities, including EMT [33, 34]. Many miRNAs, lncRNAs and circRNAs are reported to promote or suppress tumours via exosomes.

In our study, we proved that circNRIP1 sponges miR-149-5p to affect the expression level of AKT1 and eventually acts as a tumour promotor in GC. CircNRIP1 can alter metabolism and autophagy through the AKT1/mTOR axis and promote tumour metastasis through exosome communication. In conclusion, targeting circNRIP1 to explore therapeutic methods is very promising for future research.

Methods

Tissue specimens

Tumour tissues and adjacent normal stomach mucosa tissues were collected from GC patients who received

radical gastrectomy at the Department of Gastrointestinal Surgery, the First Affiliated Hospital of Nanjing Medical University, from 2013 to 2017. All patients did not receive radiotherapy and chemotherapy before surgery. All specimens were collected under the guidance of the HIPAA protocol and supervised by the ethics committee. TNM stage classification complied with the TNM classification system of the International Union Against Cancer (7th edition). We used Kaplan Meier method to draw the overall survival curve and disease-free survival curve according to the relative expression of circNRIP1 (or miR-149-5p) and the cut-off value (Median of the expression) for circNRIP1 (or miR-149-5p).

RNA-seq analysis

TRIzol reagent (Life Technologies, Carlsbad, CA, USA) was used for total RNA isolation. Approximately 3 mg of total RNA from each sample was subjected to the RiboMinus Eukaryote Kit (Qiagen, Valencia, CA) to remove ribosomal RNA before the construction of RNA-seq libraries. The NEBNext Ultra Directional RNA Library Prep Kit for Illumina (NEB, Beverly, MA, USA) was used for the preparation of strand-specific RNA-seq libraries. Briefly, approximately 50 ng of ribosome-depleted RNA sample was fragmented and then used for first- and second-strand cDNA synthesis with random hexamer primers. Second-strand cDNA synthesis was performed by adding a dUTP mix. An End-It DNA End Repair Kit was used to repair the ends of the double-stranded cDNA fragments, which were then modified by the Klenow fragment so that an A was added to the 3' end of the DNA fragments; the fragments were finally ligated to adapters. The ligated products were purified and treated with uracil DNA glycosylase (UDG) to remove second-strand cDNA. Purified first-strand cDNA was subjected to 13–15 cycles of PCR amplification, followed by library analysis with a Bioanalyser 2100 (Agilent, Santa Clara, CA, USA); the cDNA was then sequenced in a HiSeq 2000 system (Illumina, San Diego, CA, USA) on a 100-bp paired-end run.

Cell culture and treatment

The human GC cell lines BGC-823, SGC-7901, MGC-803, MKN-45, HGC-27, and AGS were used. Normal GES-1 stomach mucosa epithelium cells were purchased from the Cell Center of Shanghai Institutes for Biological Sciences. The human gastric cell line AGS was cultured in F12K medium, while the rest of the cells were cultured in RPMI 1640 medium. Both media were supplemented with 10% foetal bovine serum (Invitrogen) and 1% penicillin/streptomycin (Gibco, USA). Cells were incubated at 37 °C in a humidified atmosphere of 5% CO₂.

Oligonucleotide transfection

The human gastric cell lines MKN-45 and BGC-823 were seeded in a 6-well plate and incubated at 37 °C in humidified 5% CO₂ atmosphere overnight. CircNRIP1 siRNA, miRNA mimics and inhibitors (GenePharma, Shanghai, China) were transfected by Lipofectamine RNAiMax (Life Technologies) according to the manufacturer's protocol.

Plasmid construction and stable transfection

We synthesized human circNRIP1 cDNA and subsequently cloned it into luciferase-labelled pcDNA3.1 vector (Thermo Fisher, USA). Wild-type and mutant QKI cDNAs were synthesized and cloned into pZW1 vectors (Shanghai Institutes for Biological Sciences). In addition, MKN-45 and BGC-823 cells were transfected with the aforementioned plasmids.

RNA preparation, treatment with RNase R, and PCR

All RNAs were isolated by TRIzol reagent (Invitrogen) according to the manufacturer's protocol and then were incubated with 3 U/mg RNase R (Epicentre Technologies, USA) at 37 °C for 20 mins. These RNAs were then reverse-transcribed into cDNA by PrimeScript RT Reagent (TaKaRa, RR036A, Japan). Quantitative real-time reverse transcription polymerase chain reactions were performed on a 7500 Real-time PCR System (Applied Biosystems, Carlsbad, CA, USA) with Universal SYBR Green Master Mix (4,913,914,001, Roche, Shanghai, China). Meanwhile, we used GAPDH, β -actin and RNU6-1 as the internal references for circRNA, mRNA and miRNA, respectively.

Western blot

Protein extraction from stable transfected cells was performed by using a protein extraction kit (Key Gene, China) following the manufacturer's protocol. We measured the protein concentration by using a BCA kit (Pierce, Rockford, IL), separated protein samples via electrophoresis by using SDS-containing polyacrylamide gels, and then transferred the separated protein samples onto a polyvinylidene fluoride (PVDF) membrane (Millipore, Billerica, MA, USA). After blocking with 5% BSA in TBST buffer for 2 h, the membrane was incubated at 4 °C overnight with the primary antibody mentioned previously. Afterwards, the membrane was washed 3 times with TBST buffer for 10 min. We used a corresponding HRP-labelled secondary antibody to incubate the membrane for 2 h at room temperature and then washed 3 times with TBST buffer. Finally, blot signals were visualized by an enhanced chemiluminescence detection system with Chemiluminescence HRP Substrate (Millipore, WBKL0100).

5-Ethynyl-2'-deoxyuridine (EdU) assay

We utilized an EdU assay kit (RiboBio, China) to detect DNA synthesis and cell proliferation. We seeded 10,000 treated GC cells in a 96-well plate for one night. The next day, we added Edu solution (25 μ M) into the 96-well plate and waited for 24 h. Afterwards, we applied 4% formalin to fix the GC cells at room temperature for 2 h. In the following step, we used 0.5% TritonX-100 to permeabilize the GC cells for 10 mins and then added Apollo reaction solution (200 μ L) to stain the EdU for 30 mins and Hoechst 33342 (200 μ L) to stain the nuclei. Finally, we used a Nikon microscope (Nikon, Japan) to observe DNA synthesis and cell proliferation, reflected by red and blue signals, respectively.

Total exosome isolation

All exosome isolation (from cell culture media) reagents (4,478,359, Invitrogen) were purchased from Invitrogen (USA). The manufacturer guided us through the exosome isolation procedures. After exosomes were isolated, total RNA and protein were purified by the Total Exosome RNA and Protein Isolation Kit (4,478,545, Invitrogen).

Transmission electron microscopy (TEM)

We fixed the exosomes purified from MKN-45 and BGC-823 GC cells with 2.5% glutaraldehyde at 4 °C overnight. Subsequently, 1% OsO₄ was used to further fix the exosome samples. After the samples were fixed, we used ethanol and propylene oxide to dehydrate the exosome samples. Samples were cut into slide sections and stained with 0.3% lead citrate before we finally utilized a JEM-1010 electron microscope (JEOL, Tokyo, Japan, 2500x or 8800x magnification) to detect the exosomes.

CCK-8

The proliferation rate of MKN-45/BGC-823 cells was detected by the Cell Counting Kit-8 assay (Dojindo Laboratories, Kumamoto, Japan). Ten thousand cells were seeded in a 96-well plate, and 10 μ L of CCK-8 solution were added to each well at the same time every day. After a 2-h incubation, the absorbance at 450 nm of the experimental wells was measured with an automatic microplate reader (BioTek, Winooski, VT, USA).

Clonogenic assay

For the clonogenic assay, we seeded LV-miR-149-5p, LV-miR-149-5p-IN and LV-miR-NC GC cells in a 6-well plate (500 cells per well) for 2 weeks. All aforementioned cells in plates were then fixed in 2 mL of methanol for 30 mins and stained with crystal violet for 20 mins.

Transwell assay

The methods used for the migration assay and invasion assay were similar. We placed transwell assay inserts (Millipore, Billerica, MA, USA) in a 24-well plate. However, the difference between the methods lies in the type of membrane: The membrane in the upper transwell chamber for the invasion assay was a Matrigel-coated membrane (BD Biosciences), while that for the migration assay was a normal membrane. In the experiment, first, we placed 500 μ L of serum-free RPMI 1640 with 10% FBS in the bottom chamber. Following this, we seeded 10,000 cells in 200 μ L of RPMI 1640 in the upper chamber. After 24 to 48 h, we used methanol to fix the cells within the membrane and stained them with crystal violet. Finally, the cells were observed by microscope.

Wound-healing assay

We seeded cells in a 6-well plate and transfected and cultured them at 37 °C. We created thin scratches with a constant width along the centre of each well with a sterile pipette tip when the cells adhered to the bottom of the plate. Then, we used an inverted microscope (Olympus Optical Co., Ltd., Tokyo, Japan) to photograph images instantly (0 h) and marked the 6-well plate so that we could position the same field again. After the cells were incubated at 37 °C for 24 h, we removed the culture medium and washed the cells 3 times with PBS to remove surrounding cellular debris.

GC organoid model

Human GC organoids were constructed as described previously to simulate the microenvironment of the human body [35]. A circNRIP1 overexpression plasmid and circNRIP1 siRNA were transfected into the organoids to facilitate our investigation of the novel role played by circNRIP1 in gastric cancer progression. Human GC organoid growth was observed daily by microscope.

Fluorescence in situ hybridization

We seeded cells on glass coverslips in 12-well plates and transfected them with circNRIP1 OE and miR-149-5p mimics using Lipofectamine 2000 in MKN-45 and BGC-823 cells. Then, we washed cells with PBS and fixed them in 4% paraformaldehyde for 15 min. After cells were transfected for 48 h, we permeabilized them overnight in 70% ethanol. Next, we washed cells twice in PBS containing 5 mM MgCl₂ and rehydrated them for 10 min in 50% formamide and 2 \times SSC. We compounded a solution with 50% formamide, 0.25 mg/mL *Escherichia coli* transfer RNA, 2 \times SSC, 0.25 mg/mL salmon sperm DNA, 2.5 mg/mL BSA, and 0.5 ng/mL fluorescently labelled circNRIP1 and miR-149-5p probes, and cells were incubated in this solution at 37 °C. Three hours later, we washed cells twice for 20 min at 37 °C in 50% formamide

and $2 \times$ SSC. The following step consisted of four 5-min washes in PBS. The penultimate wash contained 4',6'-diamidino-2-phenylindole (DAPI). Finally, we washed the cells briefly with nuclease-free water.

Pull down assay

A total of 1×10^7 gastric cancer cells were harvested, lysed and sonicated. The circNRIP1 probe was used for incubation with C-1 magnetic beads (Life Technologies) at 25 °C for 2 h to generate probe-coated beads. Cell lysate with circNRIP1 probe or oligo probe was incubated at 4 °C for one night. After washing with wash buffer, the RNA mix bound to the beads was eluted and extracted with an RNeasy Mini Kit (QIAGEN) for RT-PCR or real-time PCR.

Immunofluorescence analysis

The GC cell lines were seeded on collagen-coated glass and incubated in RPMI 1640 medium at 37 °C in a humidified atmosphere of 5% CO₂ for one night. The cells were washed with PBS twice before being fixed with 4% formaldehyde and permeabilized with 0.2% Triton X-100. After being blocked with 1% BSA for 30 mins, the cells were incubated with a specific primary antibody at 4 °C for one night. The secondary antibody Cy[™] 3-Goat Anti-Rabbit IgG (Jackson, 1:100) and DAPI were successively added in a specially designed dish. After the final treatment, the cells were observed with a confocal microscope (Nikon, Japan).

Immunohistochemical (IHC) analysis

The GC tissues were fixed with 10% formalin and embedded in paraffin before the sections were treated with specific primary antibodies. After being incubated at 4 °C for one night, the sections were washed twice and subsequently incubated with HRP-polymer-conjugated secondary antibody (Abcam, UK) at room temperature. These samples were then stained with 3,3-diaminobenzidine solution and haematoxylin. Finally, we observed the slides through a microscope.

Lactate, Glucose and ATP assay

For lactate assay, we used a lactate assay kit (K627, BioVision) to detect the lactate concentration in the whole-cell lysis according to the manufacturer's instructions.

For glucose uptake assay, the indicated cells were incubated with 100 μM 2-NBDG (11,046, Cayman) 30 mins before they were washed by iced-PBS. Subsequently, we recorded the FL-1 fluorescence according to the manufacturer's instructions.

For ATP assay, we took an ATP assay kit (S0026, Beyotime) to detect intracellular ATP in whole-cell extracts by detecting the luciferase activity.

ECAR measurements

We used a Seahorse XF24 analyzer (Seahorse Biosciences) to determine the glycolytic capacity according to the manufacturer's instructions.

Haematoxylin and eosin staining of tissue

First, we used microscope slides to rehydrate the tissue samples fixed in alcohol. Subsequently, we agitated the slides for 30 s in deionized water to hydrate the tissues. The slides were then placed into a bottle filled with haematoxylin, agitated for 30 s and washed in deionized water for 30 s. After the previous steps, we used 1% eosin Y solution to stain the slides and rehydrated the samples with 95% alcohol followed by 100% alcohol. We then used xylene to extract the alcohol. In the final step, we covered the slides and observed them with a microscope.

Patient-derived xenograft models (PDX models)

First, we kept the tissues in iced RPMI 1640 with 10% foetal bovine serum, cut them into $2 \times 2 \times 3$ -mm³ pieces and then used fresh RPMI 1640 to wash the tissues twice. Before subsequent procedures, we kept the tissues in RPMI 1640 supplemented with penicillin and streptomycin. NOD/SCID mice were chosen to be the first-generation PDX mice that carried patient tissues. We used 10% chloral hydrate (0.004 mL/g) to anesthetize the mice. In a sterile operation, we buried tumour tissues in mouse backs subcutaneously while simultaneously supplementing with penicillin and streptomycin. Subsequent generations of PDX mice were BALB/c-nude mice. When each xenografted tumour tissue grew to 1–2 cm³, we followed the aforementioned protocols to harvest the tissues and immediately transplanted them into next-generation mice four times. We injected the circNRIP1 plasmids and cholesterol-conjugated circNRIP1 siRNA into tumour tissues continuously from day 0 to day 20 and then harvested the tumour tissues for further analysis on day 40.

In vivo metastasis assay

The firefly luciferase gene was stably transduced into circNRIP1 pcDNA3.1 vectors. We injected exosomes containing circNRIP1 with a luciferase label via the tail vein into BALB/c nude mice. Finally, we observed the bioluminescent signal after injecting 100 mg/kg D-luciferin (Xenogen, Hopkinton, MA) into mice by using an IVIS 100 Imaging System (Xenogen).

Dual-luciferase reporter assay

A wild-type or mut-circNRIP1 fragment was constructed and inserted downstream of the luciferase reporter gene of the pMIR-REPORT plasmid (H306, Obio Technology, Shanghai, China). We used Lipofectamine 3000 to transfect the reporter plasmid into GC cells. We then co-transfected the miR-149-5p mimic with the reporter gene into

BGC-823 and MKN-45 cells. For the last step, we used the DualLuciferase Reporter System Kit (E1910, Promega, USA) to detect firefly and renilla luciferase activity.

RNA-binding protein immunoprecipitation (RIP)

An RNA-Binding Protein Immunoprecipitation Kit (17–700, Merck, Millipore) was purchased to perform a RIP assay to determine the binding between the QKI protein and pre-mNRIP1. The procedure complied with the guidance of the manufacturer. Finally, we performed qRT-PCR on the QKI-associated RNA mixture absorbed by the magnetic beads.

Reagents and antibodies

Regarding the primary antibodies used in the study, anti-PFK (ab181861) and anti-QKI (ab126742) were purchased from Abcam (Cambridge, UK); anti-GDH was purchased from Shybio (Shanghai, China); anti-LC3A/B (12741), anti-SQSTM/p62 (8025), anti-mTOR (2983), anti-phospho-mTOR (5536,1230), anti-Akt (4685), anti-phospho-Akt (4060), anti-E-cadherin (3195), anti-N-cadherin (13116), anti-Slug (9585), anti-Snail (3879) and anti-TWSIT1 (46072) were purchased from Cell Signaling Technology (Danvers, PA USA).

Statistics

We performed our experiments in triplicate, and the results are presented as the mean value \pm standard deviation. We statistically analysed the data with Student's t-test using SPSS statistical software, and $p < 0.05$ was considered statistically significant. * indicates $p < 0.05$, ** indicates $p < 0.01$ and *** indicates $p < 0.001$.

Results

CircRNA expression profiles in gastric cancer tissues and paired normal gastric tissues

We performed RNAseq analyses of ribosomal RNA-depleted total RNA obtained from 3 clinical gastric cancer tissues and their paired adjacent normal tissues and constructed a circRNA profiling database. We detected 35,156 distinct circRNAs in all. Among them, 5528 circRNAs have been reported in circBase. The length of most circRNAs was less than 1000 nucleotides (Fig. 1). Moreover, we analysed the composition of the circRNAs in terms of gene distribution (Fig. 1b). A cluster heat map was used to show the expression variations of these circRNA transcripts in cancerous tissues relative to matched normal tissues (Additional file 4: Figure S4a). Among the 49 differentially expressed circRNAs, 33 were upregulated and 16 were downregulated in GC tissues relative to normal tissues (Fig. 1c, see Additional file 1). We focused on the most highly upregulated and downregulated circRNAs and matched them with circRNADb.Circ_0004771 (termed circNRIP1 in the remainder of the article), among

which the most highly upregulated circRNA attracted our attention. To further verify whether the expression level of circNRIP1 was high in GC tumours according to the RNA-seq data, we detected higher circNRIP1 expression in 80 GC samples relative to adjacent normal samples via qRT-PCR, which was consistent with the RNA-seq data (Fig. 1d). We next confirmed the higher levels of circNRIP1 in the SGC-7901, BGC-823, MGC-803, AGS, the MKN-45 and HGC-27 GC cell lines relative to GES-1 cells (Fig. 1e). BGC-823 cells showed the highest expression of circNRIP1, and MKN-45 cells showed the second highest expression of circNRIP1. Thus, we selected BGC-823 cells and MKN-45 GC cells to investigate the downstream regulatory pathway of circNRIP1.

Identification of the circular structure and clinical features of circNRIP1

CircNRIP1 arises from the NRIP gene, which is located at chromosome 21 and consists of the head-to-tail splicing of exon 2 and exon 3 (16386664–16,415,895) (Fig. 2a). To rule out the possibility that such head-to-tail splicing products may also derive from genomic rearrangements and trans-splicing, we first performed a qRT-PCR assay with specially designed divergent and convergent primers and discovered that circNRIP1, rather than linear-NRIP1 or actin, could resist digestion by RNase R (Fig. 2b). Moreover, we detected the expression level of back-spliced or canonical forms of NRIP1 with or without RNase R supplementation in the cDNA and gDNA of GC cells by PCR and an agarose gel electrophoresis assay (Fig. 2c). We detected circNRIP1 in cDNA with divergent primers, even under RNase R treatment. The opposite result was observed in gDNA PCR products. Additionally, the linear form of NRIP1 could not be amplified by convergent primers, demonstrating that circNRIP1 was not attributable to genomic rearrangements and PCR artefacts. Subsequently, we confirmed the head-to-tail splicing of circNRIP1 in the RT-PCR product of circHIPK3 by Sanger sequencing and also determined its genomic size and sequence as reported in the CircBase database (Fig. 2a). Furthermore, we found that circNRIP1 was more stable than linear NRIP1 in GC cells under treatment with actinomycin D, a transcription inhibitor. This result suggested that circNRIP1 can be a suitable diagnostic or prognosis marker (Fig. 2d). Furthermore, when we collected the clinical data on the aforementioned patients, we found that the expression level of circNRIP1 significantly correlated with GC tumour size and lymphatic invasion (Table 1). Additionally, we drew overall survival (OS) and disease-free survival (DFS) curves using the Kaplan-Meier method and obtained survival information for the patients we followed up previously. Patients who had high levels of circNRIP1

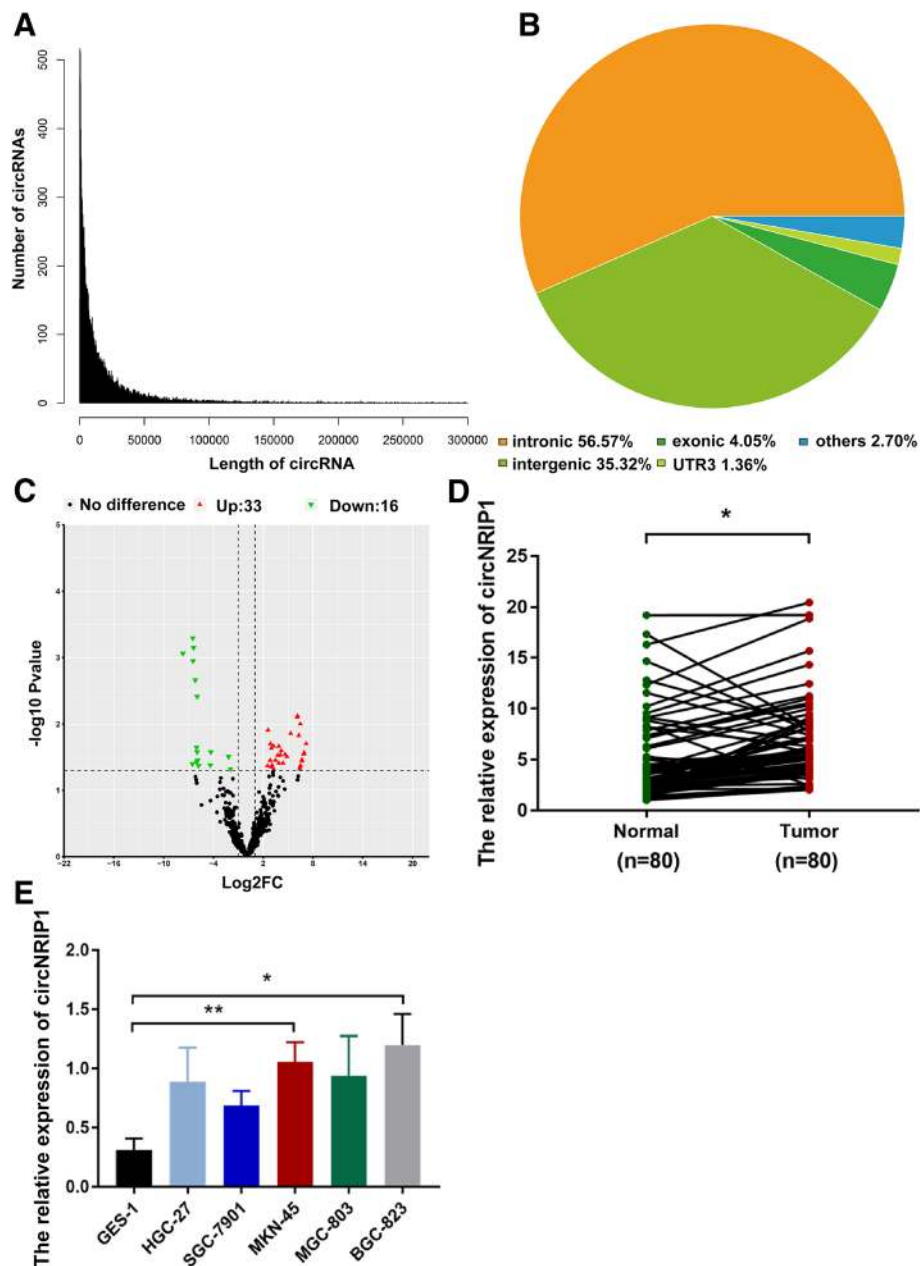


Fig. 1 CircRNA expression profiles in gastric cancer tissues and paired normal gastric tissues. **a.** The length of most circRNAs was less than 1000 nucleotides. **b.** We analysed circRNA composition in terms of gene distribution. **c.** A cluster heat map was used to show the expression variations of these circRNA transcripts in cancerous tissues relative to matched normal tissues. **d.** Volcano plots illustrated that among differentially expressed circRNAs, 33 were upregulated and 16 were downregulated in GC tissues relative to normal tissues. **e.** We detected higher circNRIP1 expression in 80 GC samples relative to adjacent normal samples via qRT-PCR. **f.** We confirmed the higher levels of circNRIP1 in the SGC-7901, BGC-823, MGC-803, AGS, MKN-45 and HGC-27 GC cell lines relative to GES-1 cells. All data are presented as the mean \pm SEM. * $p < 0.05$, ** $p < 0.01$, *** $p < 0.001$

within their GC tissues had significantly shorter overall survival (median survival of 21 months vs 51 months; $P = 0.0019$, log-rank test; Fig. 2e) and disease-free survival (median survival of 18 months vs 49 months; $P = 0.0004$, log-rank test; Fig. 2f). To summarize, circNRIP1 was confirmed to be a circular RNA and is a stable and significant

diagnostic and prognosis marker that is worthy of further exploration.

CircNRIP1 serves as a miRNA sponge of miR-149-5p

Many researchers have reported that circRNA assumes the role of a miRNA sponge in tumour development

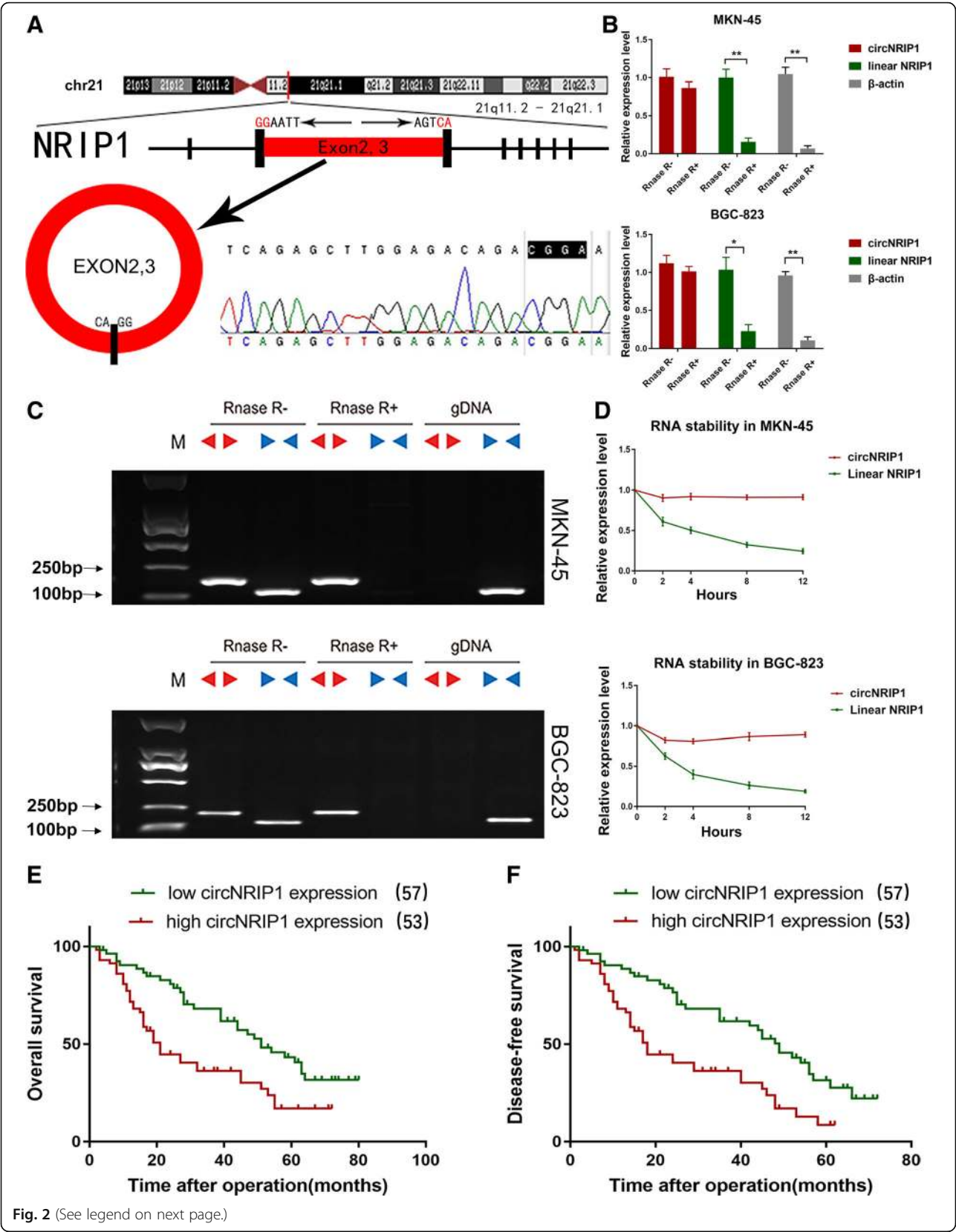


Fig. 2 (See legend on next page.)

(See figure on previous page.)

Fig. 2 Identification of the circular structure and clinical features of circNRIP1. **a.** We confirmed the head-to-tail splicing of circNRIP1 in the circHIPK3 RT-PCR product by Sanger sequencing and also determined its genomic size and sequence as reported in the CircBase database. **b.** We performed a qRT-PCR assay with specially designed divergent and convergent primers and discovered that circNRIP1, rather than linear-NRIP1 or actin, could resist digestion by RNase R. **c.** We detected the expression levels of the back-spliced and canonical forms of NRIP1 in the presence or absence of RNase R supplementation in cDNA and gDNA from GC cells by PCR and an agarose gel electrophoresis assay. **d.** We found that circNRIP1 was more stable than linear NRIP1 in GC cells under treatment with actinomycin D (a transcription inhibitor). **(e, f)** Patients who had high levels of circNRIP1 within their GC tissues had a significantly shorter overall survival (median survival of 21 months vs 51 months; $P = 0.0019$, log-rank test) and disease-free survival (median survival of 18 months vs 49 months; $P = 0.0004$, log-rank test). All data are presented as the mean \pm SEM. * $p < 0.05$, ** $p < 0.01$, *** $p < 0.001$

regulation. In addition, circRNA can further regulate downstream gene expression. We predicted the target miRNAs of circNRIP1 by cross-analysing three prediction databases: CircNet, RNA22 and RegRNA. We then selected the top 10 common miRNAs based on conjugation scores, which might indicate the potentially functional miRNAs absorbed by circNRIP1 in GC cells (Fig. 3a). A pull-down assay was used to further determine circNRIP1-associated miRNAs via a specific biotin-labelled circNRIP1 probe. We first verified the significantly upregulated pull-down efficiency of the circNRIP1 probe in a circNRIP1 overexpression plasmid (pcDNA3.1) transfected into MKN-45 and BGC-823 cells (Additional file 1: Figure S1a). We then used a qRT-PCR assay to analyse the expression levels of 10 common miRNAs predicted by 3 websites, namely hsa-miR-29b-1-5p, hsa-miR-148a-5p, hsa-miR-204-5p, hsa-miR-214-5p, hsa-miR-146a-3p, hsa-miR-149-5p, hsa-miR-148b-5p, hsa-miR-339-5p, hsa-miR-511 and hsa-miR-516b-5p, in the sponge complex from the circNRIP1 pull-down experiments in MKN-45 and BGC-823 cells. In this case, we confirmed the rich enrichment of circNRIP1 and miR-149-5p in both GC cell lines (Fig. 3b), while the other miRNAs did not show such close interactions with circNRIP1. To further verify the absorption of miR-149-5p and circNRIP1, we used a specific biotin-labelled miR-149-5p probe to successfully capture circNRIP1 relative to the NC group (Fig. 3c). Apart from the pull-down assay, we performed a dual-luciferase reporter assay to determine the direct binding between circNRIP1 and miR-149-5p based on their complementary sequences. A circNRIP1 fragment was constructed and inserted downstream of the luciferase reporter gene. Then, we co-transfected a miR-149-5p mimic with the reporter gene into BGC-823 and MKN-45 cells. A significant reduction in luciferase reporter activity was observed relative to co-transfection with control RNA (Fig. 3d). In the next phase, we

Table 1 The expression level of circNRIP1 is significantly correlated with the GC tumour size and lymphatic invasion, and the expression level of miR-149-5p is negatively correlated with the GC tumour size

Parameters	Group	circNRIP1 expression				miR-149-5p expression			
		Cases	Low	High	P-value	Cases	Low	High	P-value
Gender	female	24	11	13	0.6256	15	7	8	0.6212
	male	56	29	27		35	19	16	
Age at surgery	≥55	64	34	30	0.2636	33	17	16	0.7653
	< 55	16	6	10		17	8	9	
T grade	T1 + T2	40	22	18	0.3711	24	11	13	0.5713
	T3 + T4	40	18	22		26	14	12	
Lymphatic invasion	Negative (N0)	14	11	3	0.0186*	15	5	10	0.1228
	Positive (N1-N3)	66	29	37		35	20	15	
Tumor site	Cardiac	30	21	9	0.1689	18	7	11	0.2386
	Non-cardiac	50	19	31		32	18	14	
Stage	I-II	43	24	19	0.2622	23	11	12	0.7766
	III-IV	37	16	21		27	14	13	
Size(cm)	< 3	37	23	14	0.0436*	24	8	16	0.0235*
	≥3	43	17	26		26	17	9	
Histology grade	Well-moderately	28	13	15	0.6392	16	7	9	0.5443
	Poorly-signet	52	27	25		34	18	16	

All data are presented as the mean \pm SEM. * $p < 0.05$, ** $p < 0.01$, *** $p < 0.001$

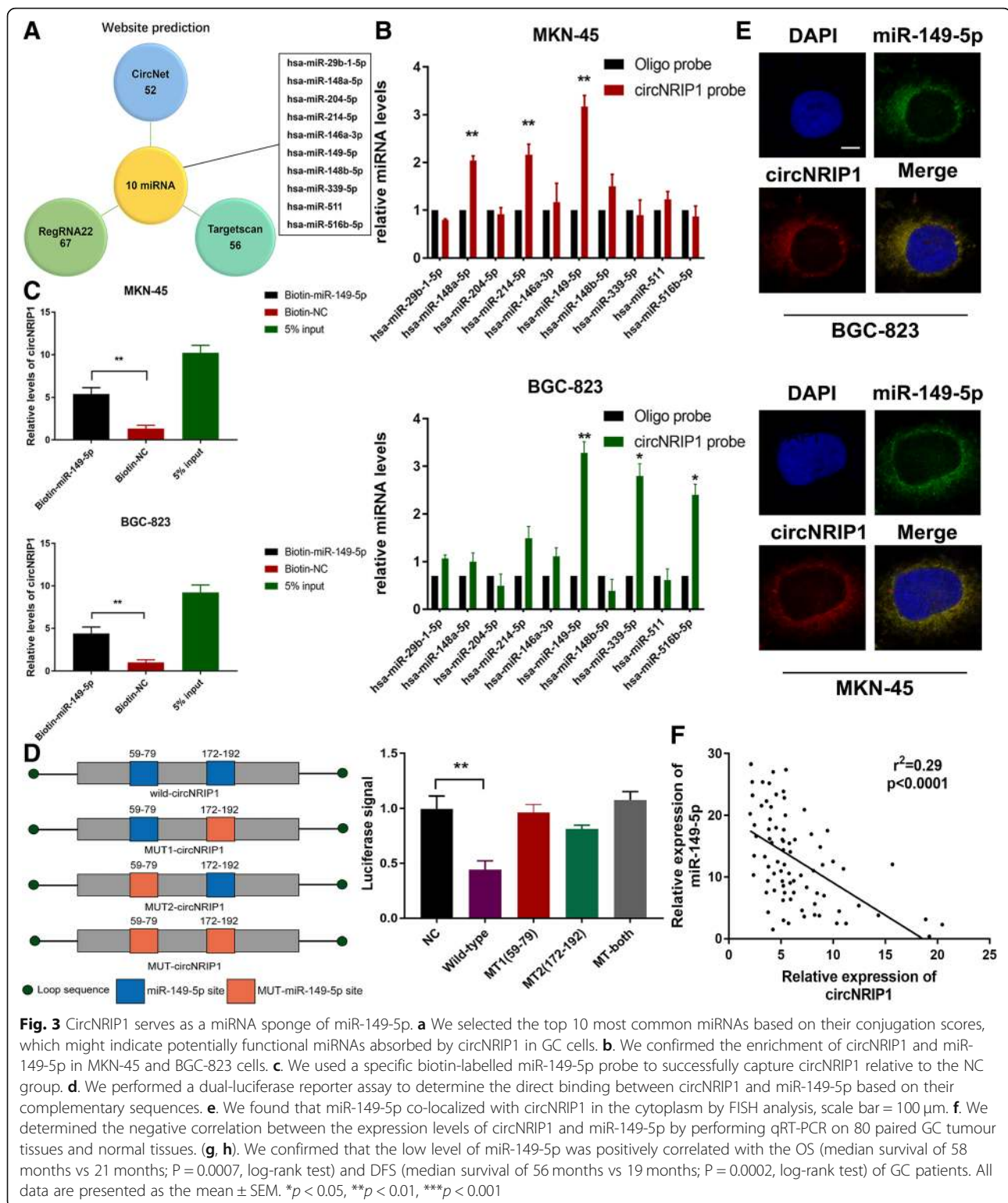


Fig. 3 CircNRIP1 serves as a miRNA sponge of miR-149-5p. **a** We selected the top 10 most common miRNAs based on their conjugation scores, which might indicate potentially functional miRNAs absorbed by circNRIP1 in GC cells. **b** We confirmed the enrichment of circNRIP1 and miR-149-5p in MKN-45 and BGC-823 cells. **c** We used a specific biotin-labelled miR-149-5p probe to successfully capture circNRIP1 relative to the NC group. **d** We performed a dual-luciferase reporter assay to determine the direct binding between circNRIP1 and miR-149-5p based on their complementary sequences. **e** We found that miR-149-5p co-localized with circNRIP1 in the cytoplasm by FISH analysis, scale bar = 100 μ m. **f** We determined the negative correlation between the expression levels of circNRIP1 and miR-149-5p by performing qRT-PCR on 80 paired GC tumour tissues and normal tissues. **(g, h)** We confirmed that the low level of miR-149-5p was positively correlated with the OS (median survival of 58 months vs 21 months; $P = 0.0007$, log-rank test) and DFS (median survival of 56 months vs 19 months; $P = 0.0002$, log-rank test) of GC patients. All data are presented as the mean \pm SEM. * $p < 0.05$, ** $p < 0.01$, *** $p < 0.001$

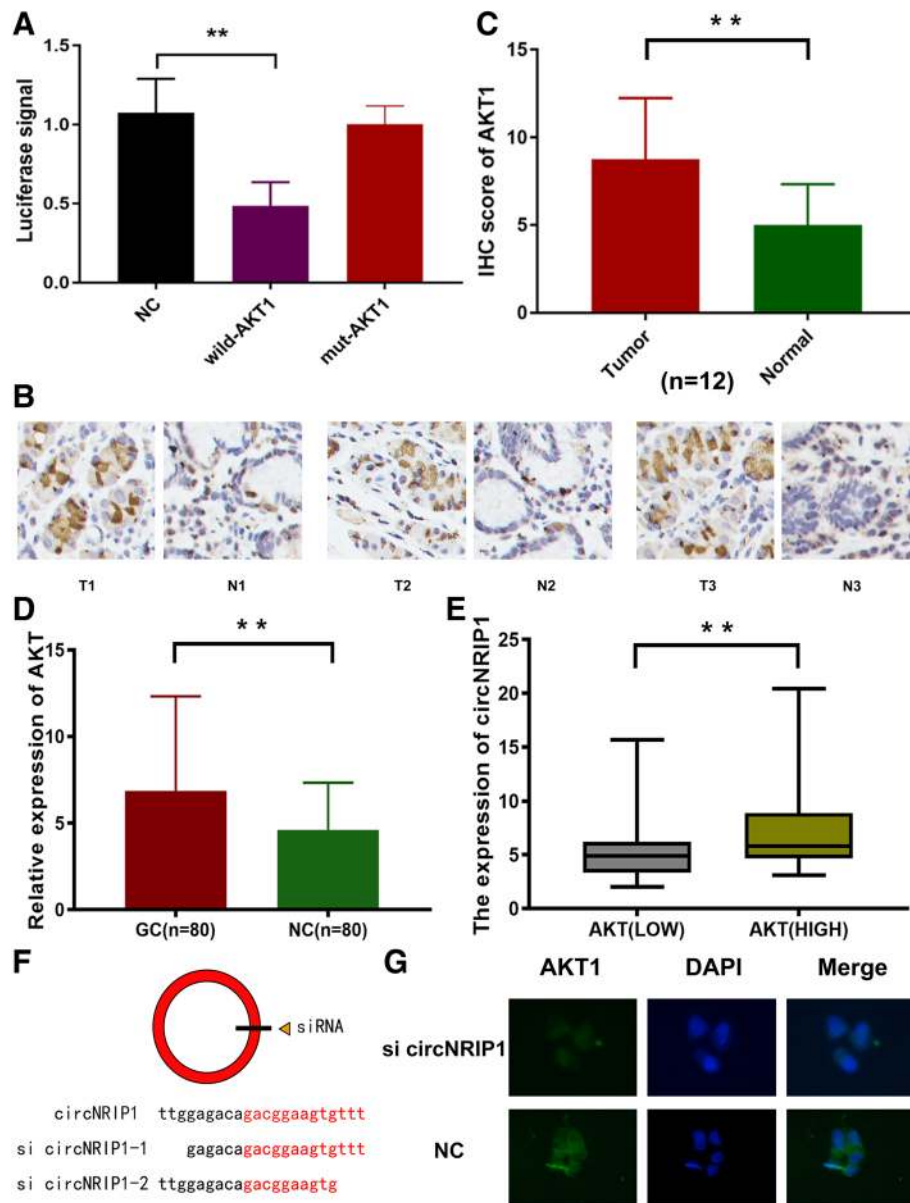


Fig. 4 Knockdown of circNRIP1 reduces the expression of AKT1. **a.** We performed a dual-luciferase reporter assay to determine the direct binding between 149-5p and AKT1 in GC cells. **b.** We found that AKT1 was significantly upregulated in GC tissues (415 GC tissues vs 34 normal tissues), and patients with high levels of AKT1 (298 GC tissues vs 94 normal tissues) had lower OS based on an analysis of the TCGA database. **c, d.** We subsequently detected higher levels of AKT1 in GC tissues than in adjacent normal tissues by performing immunochemistry analysis on 12 paired GC tumour tissues and normal stomach tissues, scale bar = 200 μ m. **e.** qRT-PCR further confirmed the expression level of AKT1 and showed that it was upregulated in 80 GC tissues relative to adjacent normal tissues. **f.** We detected the circNRIP1 level in both groups and determined that the level of circNRIP1 in the high AKT1 group (n = 40) was significantly higher than that in the low AKT1 group (n = 40). **g.** Two circNRIP1 small interfering RNAs (siRNAs) specifically targeting the backsplice junction sequences at different binding sites in circNRIP1 were designed. **h.** Immunofluorescence assay showed that circNRIP1 knockdown successfully inhibited the expression level of AKT1, scale bar = 50 μ m. All data are presented as the mean \pm SEM. * p < 0.05, ** p < 0.01, *** p < 0.001

mutated two binding sites in the 3'UTR of the circNRIP1 sequence. We found that co-transfection of miR-149-5p and mut-circNRIP1, with either one of the two binding sites or both mutated, did not induce a significant reduction in the luciferase signal (Fig. 3d, Additional file 5: Figure S5a). Therefore, the direct

interaction of circNRIP1 and miR-149-5p was confirmed. FISH analysis was performed in BGC-823 and MKN-45 cells, and we found that miR-149-5p was co-localized with circNRIP1 in the cytoplasm, which further suggested an interaction between circNRIP1 and miR-149-5p (Fig. 3e). Furthermore, we determined the

negative correlation between the expression level of circNRIP1 and miR-149-5p by performing qRT-PCR on 80 paired GC tumour tissues (Fig. 3f). Many reports have described the tumour suppressor role of miR-149-5p in various cancers [36, 37], which allowed us to determine the role of miR-149-5p in gastric cancer. We detected that overexpression of miR-149-5p in MKN-45 and BGC-823 cells blocked the proliferation rate (Additional file 1: Figure S1b), DNA synthesis (Additional file 1: Figure S1c), migration and invasion (Additional file 1: Figure S1d) abilities of GC cells, while miR-149-5p reduction had the opposite effects on GC cells. Furthermore, we collected clinical data from the aforementioned patients and found that the expression level of miR-149-5p was negatively correlated with GC tumour size (Table 1). We then used GC tissues from patients who were followed up for a period of time to verify the expression of miR-149-5p and used the Kaplan-Meier Plotter method to draw overall survival (OS) and disease-free survival (DFS) curves based on the median expression of miR-149-5p (Additional file 5: Figure S5b). Thus, we confirmed that a high level of miR-149-5p was positively correlated with the OS (median survival of 58 months vs 21 months; $P = 0.0007$, log-rank test; Additional file 5: Figure S5b) and DFS (median survival of 56 months vs 19 months; $P = 0.0002$, log-rank test; Additional file 5: Figure S5b) of GC patients. In conclusion, it is suggested that circNRIP1 can serve as a sponge of miR-149-5p in the cytoplasm within GC cells, and the high level of miR-149-5p is positively correlated with the survival of GC patients.

Knockdown of circNRIP1 reduces the expression of AKT1

It has been reported that miR-149-5p can inhibit cell proliferation, invasion and migration in human hepatocellular carcinoma by targeting AKT1 and further facilitating the mTOR pathway [38]. The interaction between miR-149-5p and AKT1 is also reported in colon carcinoma and glioblastoma [39, 40]. Based on the assumption that circNRIP1 plays a tumour promoter role in GC through the classic ceRNA mechanism, we tried to identify the ceRNA of circNRIP1, which should also be the downstream target gene of miR-149-5p. Herein, we performed a dual-luciferase reporter assay to determine the direct binding between 149-5p and AKT1 in GC cells. The wild-type (wild-AKT1) and mutant AKT1 (mut-AKT1) reporter genes were constructed as described in the aforementioned reports. Then, we co-transfected a miR-149-5p mimic with the reporter genes into BGC-823 and MKN-45 cells. A significant reduction in luciferase reporter activity was observed relative to co-transfection with control RNA (Fig. 4a). Moreover, we found that co-transfection of miR-149-5p and mut-AKT1 did not induce a significant reduction in

the luciferase signal (Fig. 4a). To validate the ceRNA analysis, we made an effort to verify the specific tumour expression and prognostic role of AKT1 in gastric cancer among a large number of patients by analysing the TCGA database. We found that AKT1 was significantly upregulated in GC tissues (415 GC tissues vs 34 normal tissues), and patients with high levels of AKT1 (298 GC tissues vs 94 normal tissues) had a lower OS (Additional file 5: Figure S5c). To verify the aforementioned expression pattern of AKT1 in GC tissues, we subsequently detected higher levels of AKT1 in GC tissues than in adjacent normal tissues by performing immunohistochemistry analysis on 12 paired GC tumour tissues and paired normal stomach tissues (Fig. 4b, c). qRT-PCR further confirmed the expression level of AKT1 and showed that it was upregulated in 80 GC tissues relative to adjacent normal tissues (Fig. 4d). Next, we wanted to determine whether circNRIP1 is co-expressed with AKT1, and we sorted the 80 GC tissue samples into a low AKT1 group ($n = 40$) and a high AKT1 expression group ($n = 40$) based on the median expression of AKT1. Then, we detected the circNRIP1 level in two groups and found that the level of circNRIP1 in the high AKT1 group was significantly higher than that in the low AKT1 group (Fig. 4e). To further analyse the regulatory role of circNRIP1 on AKT1, we designed two circNRIP1 small interfering RNAs (siRNAs) to specifically target the backsplice junction sequence at different binding sites of circNRIP1 (Fig. 4f). We knocked down circNRIP1 expression in MKN-45 and BGC-823 cells by using circNRIP1 siRNA. The efficiency of circNRIP1 silencing was confirmed by qRT-PCR (Additional file 2: Figure S2a). To rule out the possibility that circNRIP1 siRNA might exert effects on the mRNA level of NRIP1 (linear NRIP1), we analysed the NRIP1 mRNA level and found no significant changes (Additional file 2: Figure S2a). Then, we chose si-circNRIP1-1 to perform further experiments based on its higher knockdown efficiency. We detected lower expression levels of AKT1 by qRT-PCR after knocking down circNRIP1 in MKN-45 and BGC-823 GC cells (Additional file 2: Figure S2b). Finally, an immunofluorescence assay was utilized to observe AKT1 expression in human GC organoid models. The outcomes showed that circNRIP1 knockdown successfully inhibited the expression level of AKT1 (Fig. 4g). Thus, we proved the positive regulation of the ceRNA AKT1 by circNRIP1.

Knockdown of circNRIP1 inhibits the proliferation, migration and invasion of GC cells in vitro

As we previously proved that knockdown of circNRIP1 significantly inhibits AKT1 expression in GC cells, we hypothesized that blocking the expression of circNRIP1 might reduce the survival abilities of GC cells in terms of proliferation and metastasis. Based on this hypothesis, we transfected the circNRIP1 siRNA and circNRIP1

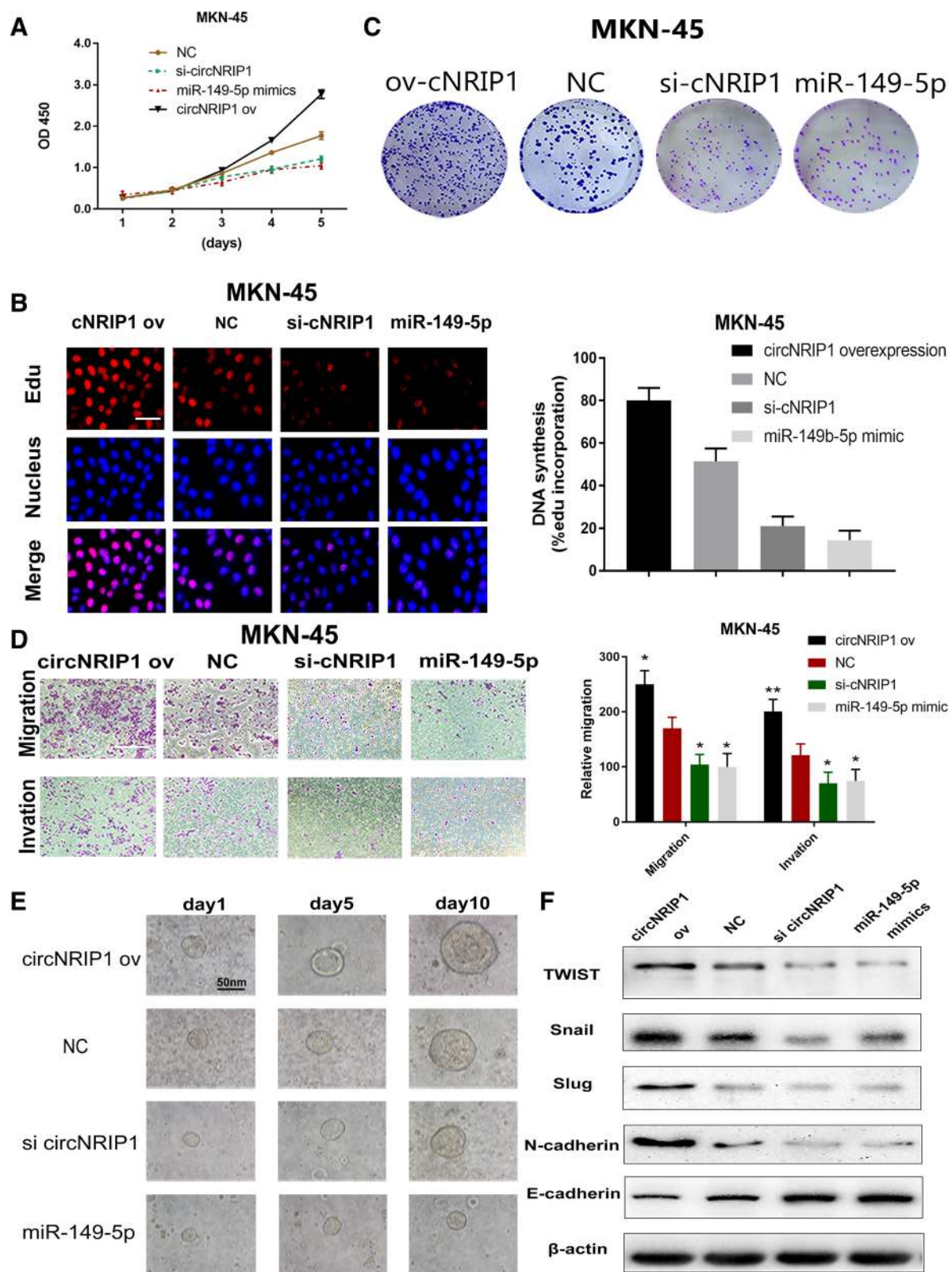


Fig. 5 (See legend on next page.)

(See figure on previous page.)

Fig. 5 Knockdown of circNRIP1 inhibits the proliferation, migration and invasion of GC cells in vitro. **a.** We observed that circNRIP1 silencing significantly inhibited the cell proliferation rate, as indicated by the CCK8 assay, and overexpression of circNRIP1 exerted the opposite effect on the GC cell proliferation rate. **b.** We observed that circNRIP1 silencing significantly inhibited DNA synthesis, as determined by the Edu assay, and overexpression of circNRIP1 exerted the opposite effect on GC cell DNA synthesis as indicated by the EDU assay, scale bar = 100 μ m. **c.** We observed that circNRIP1 silencing significantly inhibited colony formation ability, and overexpression of circNRIP1 exerted the opposite effect on colony formation. **d.** Knockdown of circNRIP1 successfully reduced the migration and invasion ability of GC cells, and overexpression of circNRIP1 exerted the opposite effect on metastasis, as indicated by the transwell assay, scale bar = 200 μ m. **e.** We observed that both circNRIP1 knockdown and miR-149-5p overexpression significantly inhibited the growth of the organoid models, while circNRIP1 overexpression promoted organoid model survival. **f.** We detected downregulation of the mesenchymal cell markers TWIST, snail, slug, and N-cadherin and upregulation of the epithelial cell marker E-cadherin in human GC organoid models when we knocked down circNRIP1 or overexpressed miR-149-5p. All data are presented as the mean \pm SEM. * p < 0.05, ** p < 0.01, *** p < 0.001

overexpression plasmid into MKN-45 and BGC-823 cells. In the following steps, CCK8, Edu and colony formation assays were performed to determine the proliferation ability of GC cells, and the metastasis ability of GC cells was measured by a transwell assay and wound healing assay. We observed that circNRIP1 silencing significantly inhibited the cell proliferation rate as indicated by the CCK8 assay (Fig. 5a, Additional file 6: Figure S6b), DNA synthesis as determined by the Edu assay (Fig. 5b, Additional file 6: Figure S6c), and the colony formation ability (Fig. 5c, Additional file 6: Figure S6a) of MKN-45 and BGC-823 cells. In addition, knockdown of circNRIP1 successfully reduced the migration and invasion of GC cells (Fig. 5d, Additional file 2: Figure S2c, Additional file 6: Figure S6d). However, overexpression of circNRIP1 exerted the opposite effect on GC cell proliferation and metastasis (Fig. 5a, b, c, d, Additional file 2: Figure S2c, Additional file 6: Figure S6a-d). We assumed that miR-149-5p overexpression phenocopied the tumour-suppressor effects of circNRIP1 silencing in MKN-45 and BGC-823 cells. To verify our assumption, we then transfected GC cells with a miR-149-5p mimic, and both the sequence and transfection efficiency were confirmed by qRT-PCR (Additional file 2: Figure S2d).

We found that miR-149-5p overexpression almost phenocopied the biological effects of circNRIP1 knockdown on GC cell proliferation and metastasis (Fig. 5a, b, c, d, Additional file 2: Figure S2c, Additional file 6: Figure S6a-d). Finally, we built human GC organoid models to investigate the biological functions of circNRIP1 and miR-149-5p. We observed that both circNRIP1 knockdown and miR-149-5p overexpression significantly inhibited the growth of the organoid models, while circNRIP1 overexpression promote its growth (Fig. 5e, Additional file 6: Figure S6e). Epithelial-mesenchymal transition (EMT) is recognized as an important mechanism mediating the initiation and promotion of metastasis in GC [41, 42]. We already determined the relation between circNRIP1 and GC metastasis in vitro and the positive regulation of AKT1 by circNRIP1. Many reports have described the promoting role of the PI3K/AKT signalling pathway on EMT via

upregulation of the expression of the transcription factor TWIST and the DNA-binding proteins snail and slug [43, 44]. We detected the downregulation of the mesenchymal cell markers TWIST, snail, slug, and N-cadherin and the upregulation of the epithelial cell marker E-cadherin in human GC organoid models when we knocked down circNRIP1 or overexpressed miR-149-5p (Fig. 5f). Conversely, circNRIP1 overexpression increased the expression levels of mesenchymal cell markers and reduced the expression level of the epithelial cell marker (Fig. 5f). Thus, the miRNA sponge role of circNRIP1 was further confirmed because miR-149-5p inhibitors could phenocopy the biological function of circNRIP1 overexpression. In summary, we proved that circNRIP1 knockdown could inhibit the proliferation, migration and invasion of GC cells and block the growth of human GC organoid models. CircNRIP1 functions as a tumour suppressor by sponging miR-149-5p, which remains to be explored in depth.

The circNRIP1-miR-149-5p-AKT1/mTOR axis is responsible for the altered metabolism in GC cells and promotes GC development

To verify whether circNRIP1 plays a tumour promotor role via the AKT/mTOR pathway by sponging miR-149-5p, we attempted to detect the expression level of AKT1, the target of miR-149-5p, in GC cells. MiR-149-5p inhibitors were used to examine whether the therapeutic effects of circNRIP1 knockdown could be reversed by knocking down miR-149-5p. The sequence and transfection efficiency of miR-149-5p inhibitors were confirmed by qRT-PCR (Additional file 2: Figure S2d). Subsequently, we found that knockdown of circNRIP1 and miR-149-5p significantly reversed the downregulated expression levels of AKT1, p-AKT1, mTOR and p-mTOR in MKN-45 and BGC-823 cells relative to circNRIP1 inhibition (Fig. 6a, Additional file 7: Figure S7a). We attempted to determine whether the biological function of circNRIP1 in GC cells could also be reversed by miR-149-5p inhibitors. We observed that the reduced proliferation indicated by the Edu assay

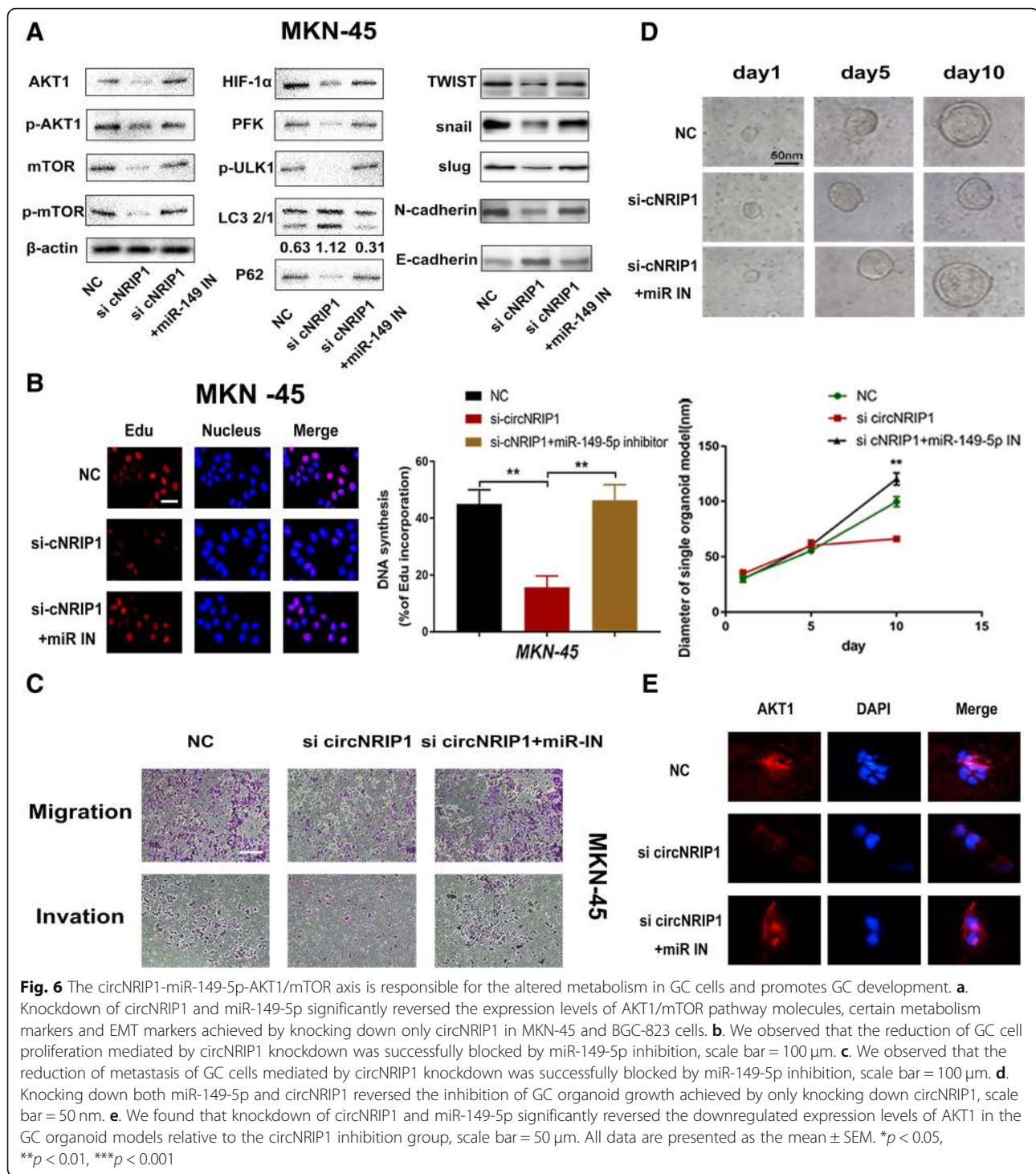


(Fig. 6b, Additional file 7: Figure S7b) and reduced metastasis indicated by the transwell assay (Fig. 6c, Additional file 7: Figure S7c) in GC cells mediated by circNRIP1 knockdown were successfully restored by miR-149-5p inhibition. Additionally, the GC organoid models were further used to investigate the circNRIP1/miR-149-5p regulatory role in tumour

growth. We found that knocking down miR-149-5p and circNRIP1 could reverse the inhibited growth of the GC organoids achieved by only knocking down circNRIP1 (Fig. 6d).

In the next step, we tried to understand the deeper tumour promotor mechanism underlying the circNRIP1/miR-149-5p/AKT1/mTOR axis. Thus, we

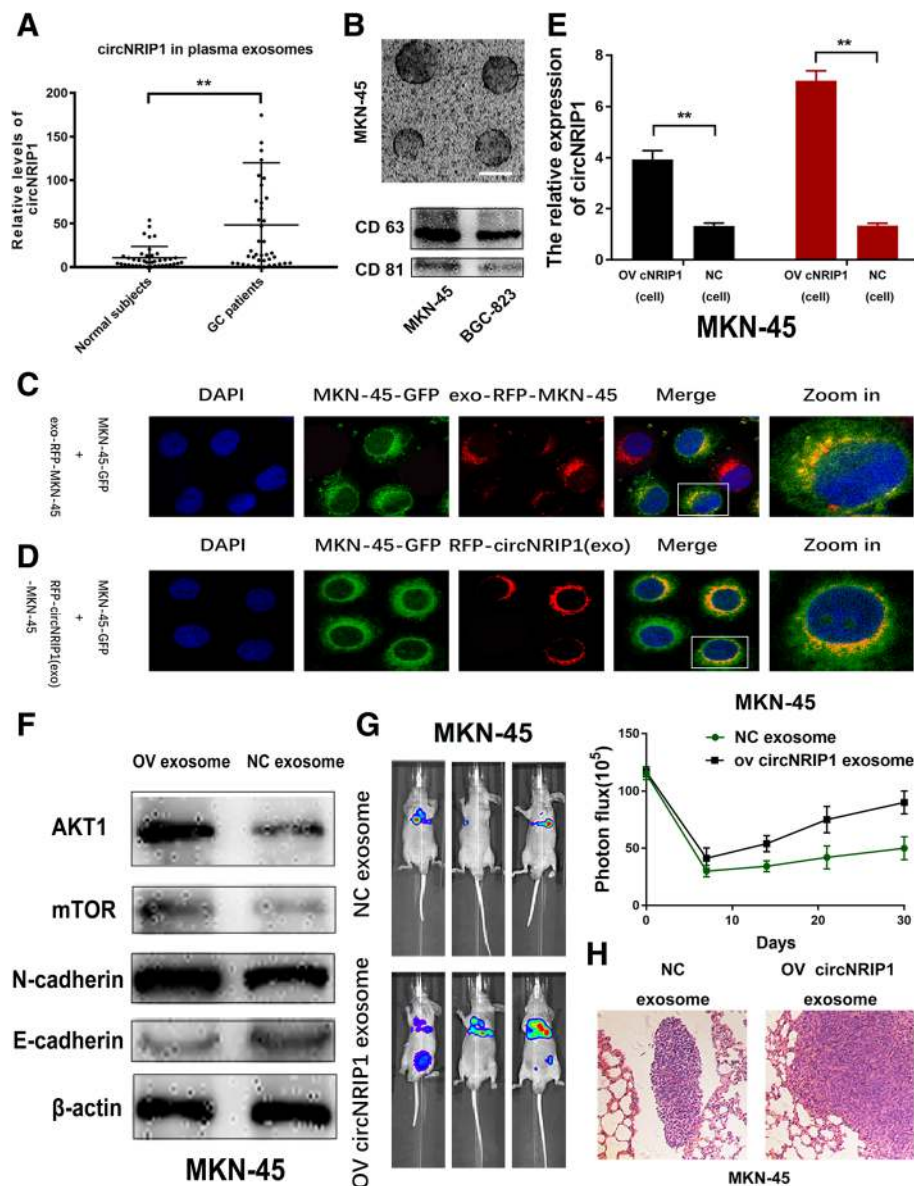


Fig. 7 Exosomal circNRIP1 regulates AKT1 expression as well as EMT in vitro and promotes metastasis in vivo. **a.** We determined the significantly higher expression level of circNRIP1 in plasmatic exosomes from GC patients by qRT-PCR. **b.** We used a transmission electron microscope (TEM) to determine the existence and morphology of exosomes purified from GC cell medium (exosome-free FBS), scale bar = 25 μm. We further confirmed the exosomes by detecting protein markers, including CD63 and CD81, by western blot. **c.** Red exosome signals were found in the cytoplasm of GFP-labelled tumour cells when exo-RFP GC cells were mixed with the same amount of GFP-labelled GC cells for 72 h, scale bar = 50 μm. **d.** We then purified exosomes and added them into GFP-labelled MKN-45 or BGC-823 GC cells. The red signal of circNRIP1 similarly appeared in the cytoplasm of GFP-labelled GC cells after 72 h, scale bar = 50 μm. **e.** We performed qRT-PCR and detected higher circNRIP1 expression in exosomes purified from circNRIP1-overexpressing GC cells relative to those from NC cells. **f.** We detected upregulated AKT1, mTOR and EMT markers in GC cells by co-culturing them with exosomes of OV circNRIP1 GC cells (OV exosomes) for 72 h via western blot. **g.** According to the luciferase intensities detected in the thoracic cavity, we found that GC cells treated with OV exosomes showed higher metastasis potential. **h.** We harvested lung tissues for H&E staining to characterize the cancerous nodes. Cancerous node size was consistent with luciferase intensity, scale bar = 200 μm. All data are presented as the mean ± SEM. **p* < 0.05, ***p* < 0.01, ****p* < 0.001

detected the expression levels of mTORC1, HIF1α, PFK, p-ULK, LC3, and P62 in GC cells. To test our hypothesis that circNRIP1 could modulate the Warburg effect via miR-149-5p, we performed a series of glycolysis detection experiments. We found that knockdown of

circNRIP1 reduced the lactate contents, glucose uptake and ATP production in MKN-45 and BGC-823 cells. However, the reduction in glycolysis activity could be restored when we knocked down both circNRIP1 and miR-149-5p (Additional file 3: Figure S3a, b, c). To

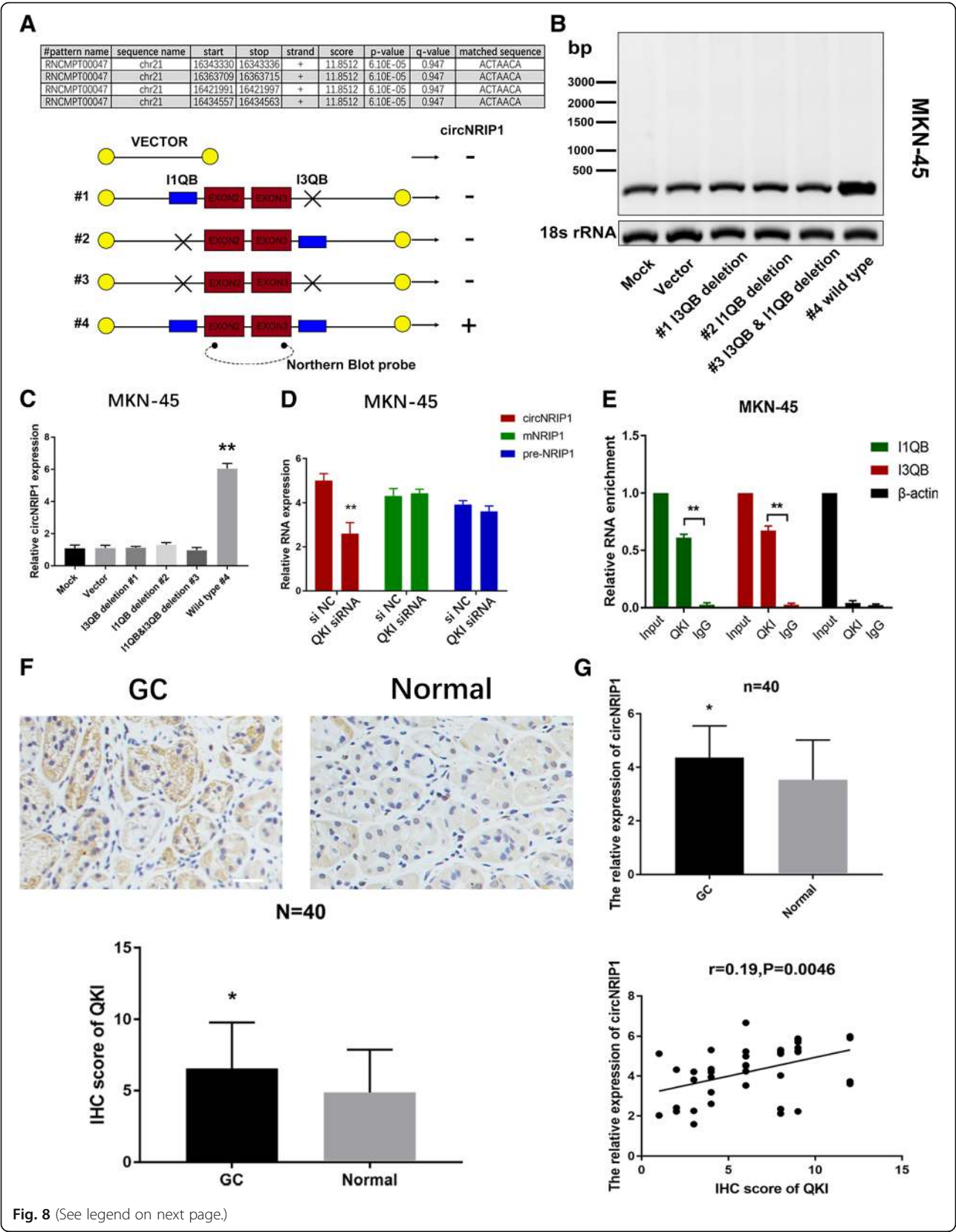


Fig. 8 (See legend on next page.)

(See figure on previous page.)

Fig. 8 Expression of circNRIP1 in GC can be regulated by QKI. **a.** We constructed a series of mutation plasmids (pZW1) consisting of either mutated I1QB or I3QB (#1, #2) or both I1QB and I3QB (#3), and we also constructed a wild-type plasmid spanning intron 1 to intron 3 (#4). **b.** We observed that only the wild-type plasmid (#4), and neither the I1QB nor I3QB deletion constructs (#1–3), could overexpress circNRIP1 according to northern blotting of GC cells. **c.** We observed that only the wild-type plasmid (#4), and neither the I1QB nor I3QB deletion constructs (#1–3), could overexpress circNRIP1 according to qRT-PCR in GC cells. **d.** We knocked down QKI and observed a significant reduction in circNRIP1 but not pre-mNRIP1 or mNRIP1. **e.** Enrichment of I1QB and I3QB was observed when we used an antibody against QKI. **f.** We detected higher QKI expression level in GC tumour tissues relative to adjacent normal stomach tissues among 40 patients by immunohistochemistry, scale bar = 200 μ m. **g.** We performed qRT-PCR on these 40 patients and discovered that the expression level of circNRIP1 was positively related to the QKI histochemistry score. All data are presented as the mean \pm SEM. * $p < 0.05$, ** $p < 0.01$, *** $p < 0.001$

further verify the regulatory role of circNRIP1 in glycolysis via miR-149-5p, the extracellular acidification rate (ECAR) was measured. As expected, knockdown of both miR-149-5p and circNRIP1 rescued the reduced glycolysis rate and glycolytic capacity achieved when knocking down only circNRIP1 (Additional file 3: Figure S3d). The aforementioned results indicate that circNRIP1 could regulate cellular metabolism, particularly glycolysis, via miR-149-5p. Additionally, we previously proved that circNRIP1 could promote the metastasis of GC cells via EMT. Thus, we also investigated the aforementioned EMT markers under treatment with miR-149-5p inhibitors and circNRIP1 siRNA. We found that knockdown of circNRIP1 could downregulate the above anabolism targets and mesenchymal cell markers, while co-transfection with a miR-149-5p inhibitor could abolish the aforementioned results (Fig. 6a, Additional file 7: Figure S7a). Furthermore, we found that knockdown of circNRIP1 could upregulate autophagy and epithelial cell markers, while co-transfection with a miR-149-5p inhibitor could abolish the aforementioned results (Fig. 6a, Additional file 7: Figure S7a). In the next step, we performed an immunofluorescence assay to detect the AKT1 expression level in GC organoid models. We found that knockdown of both circNRIP1 and miR-149-5p significantly reversed the down-regulated expression levels of AKT1 in the GC organoid models relative to circNRIP1 inhibition (Fig. 6e).

Together, we proved that circNRIP1 promotes GC progression as a sponge of miR-149-5p through AKT/mTOR-mediated metabolism and the EMT pathway.

Exosomal circNRIP1 regulates AKT1 expression as well as EMT in vitro and promotes metastasis in vivo

First, we hypothesized that there is exosomal communication between GC cells. To verify our assumption, we purified exosomes in plasma from 40 GC patients and 40 normal subjects, and we determined the significantly higher expression level of circNRIP1 in plasmatic exosomes from GC patients (Fig. 7a). Next, we used a transmission electron microscope (TEM) to determine the existence and morphology of exosomes purified from GC cell medium (exosome-free FBS) (Fig. 7b). We further confirmed the exosomes by detecting protein

markers, including CD63 and CD81, through western blotting (Fig. 7b).

To trace the exosome communication between GC cells under more realistic conditions, we established a co-cultivation system and transfected an RFP-tagged CD63 plasmid into MKN-45 and BGC-823 cells (exo-RFP-MKN-45 and exo-RFP-BGC-823) to label the exosomes within tumour cells. Red exosome signal was found in the cytoplasm of GFP-labelled tumour cells when exo-RFP GC cells were mixed with the same amount of GFP-labelled GC cells for 72 h (Fig. 7c, Additional file 8: Figure S8b). These results prove that exosomes could be used as a communication tool between GC cells. To further validate the ability of circNRIP1 to assemble into exosomes, we transfected an RFP-tagged circNRIP1-overexpressing plasmid into MKN-45 and BGC-823 cells and then purified and added exosomes into GFP-labelled MKN-45 or BGC-823 GC cells. The red signal of circNRIP1 similarly appeared in the cytoplasm of GFP-labelled GC cells after 72 h (Fig. 7d, Additional file 8: Figure S8c). We detected higher circNRIP1 expression in exosomes purified from circNRIP1-overexpressing GC cells relative to those from NC cells (Fig. 7e, Additional file 8: Figure S8d). These results all proved that circNRIP1 could enter into exosomes from GC cells.

Subsequently, we detected upregulated AKT1, mTOR and EMT markers in GC cells by co-culturing them with exosomes of OV circNRIP1 GC cells (OV exosomes) for 72 h via western blotting (Fig. 7f, Additional file 8: Figure S8e). We considered recent reports describing the positive correlation between exosomal communication and metastasis. Additionally, we proved that circNRIP1 functions as a promoter of EMT. We attempted to detect the role of exosomal circNRIP1 in distant metastasis via tail vein injection of GC cells co-cultured with OV exosomes and NC exosomes into BALB/c nude mice. We observed mostly lung metastases and a few peritoneal metastases by detecting luciferase intensities every week for four weeks. According to the luciferase intensities detected in the thoracic cavity, we found that GC cells treated with OV exosomes showed higher metastasis potential (Fig. 7g, Additional file 8: Figure S8f). Next, we harvested lung tissues for H&E staining (Fig. 7h,

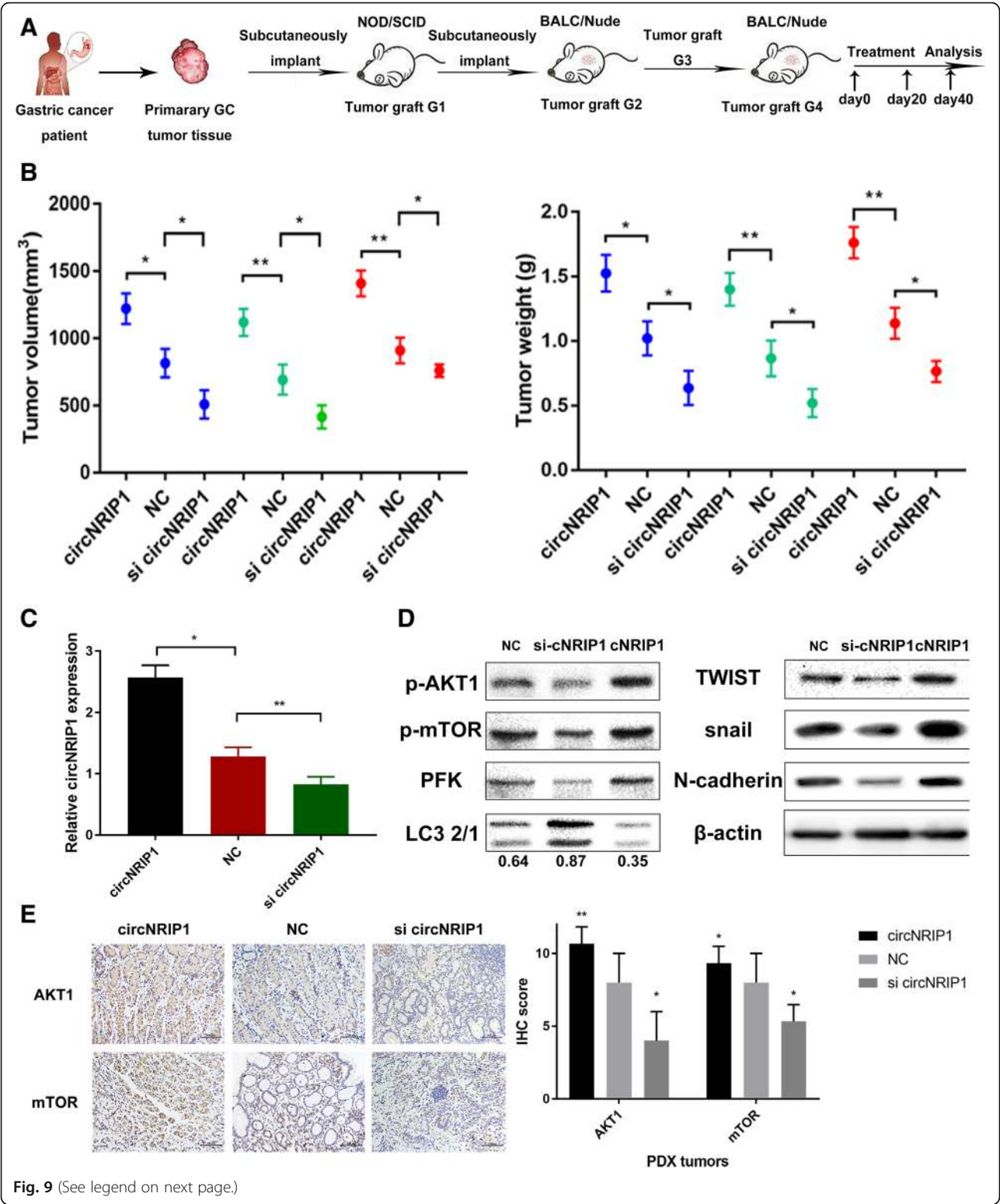


Fig. 9 (See legend on next page.)

(See figure on previous page.)

Fig. 9 CircNRIP1 plays a tumour promotor role during GC growth in vivo. **a.** The circNRIP1 overexpression plasmid and cholesterol-conjugated circNRIP1 siRNA were continuously injected intratumorally into PDX mice. **b.** The donor patients were clinically characterized. **c.** The engrafted tumours were histopathologically analysed, scale bar = 100 μ m. **d.** We found that circNRIP knockdown in vivo significantly blocked tumour growth in terms of tumour weight and volume relative to the negative control group, whereas overexpression of circNRIP1 promoted the growth of xenografted tumours. **e.** qRT-PCR was performed in PDX tumours, and we found increased and persistent levels of circNRIP1 in the circNRIP1 overexpression plasmid-treated groups relative to the NC group and lower levels of circNRIP1 in the long-term circNRIP1 siRNA-treated groups. **f.** The expression levels of p-AKT1, p-mTOR, PFK, LC3 and EMT markers were observed in PDX tumour tissues by western blotting. **g.** The expression levels of AKT1 and mTOR were again observed in PDX tumours by IHC, scale bar = 100 μ m. All data are presented as the mean \pm SEM. * p < 0.05, ** p < 0.01, *** p < 0.001

Additional file 8: Figure S8g) to characterize the cancerous nodes in lung tissues. Cancerous node size was consistent with luciferase intensity.

In summary, we proved the role of circNRIP1 in promoting EMT and metastasis in vivo via exosomal communication.

The expression of circNRIP1 in GC can be regulated by QKI

The majority of circRNAs originate from exons flanked with introns. CircRNA formation was reported to be regulated by several RNA binding proteins targeting specific sequence motifs within the flanking introns. When bound to RNA-binding proteins, the aforementioned sequences are entwined into RNA duplexes and then undergo back-splicing editing to finally become circRNAs [45, 46]. Thus, we assumed that circNRIP1 formation is controlled under a similar mechanism. Quaking (QKI) is one of the RNA binding proteins reported to be a major regulator of circRNA biogenesis in EMT [47]. Considering the promotor role of circNRIP1 in EMT, we attempted to determine whether QKI could target specific binding sequences within NRIP1 pre-mRNA to promote circNRIP1 formation.

With circNRIP1 derived from exon 2 and exon 3, we first aligned flanking intron 1 and intron 3 of the NRIP1 gene to the known QKI binding motif and found four canonical QKI binding sequences. Two were located upstream, while the other two were located downstream of the circNRIP1-forming splice sites (Fig. 8a). We designated these binding sequences as I1QB (intron 1 QKI binding sequences), encompassing the two upstream QKI binding sites, and I3QB (intron 3 QKI binding sequences), including the two downstream QKI binding sites. Subsequently, we constructed a series of mutation plasmids (pZW1) by either mutating I1QB or I3QB (#2,#1) or mutating both I1QB and I3QB (#3), and we also constructed a wild-type plasmid spanning intron 1 to intron 3 (#4) to verify whether circNRIP1 was promoted by I1QB and I3QB (Fig. 8a). We observed that only the wild-type plasmid (#4), not the I1QB and I3QB deletion constructs (#1–3), could overexpress circNRIP1 by northern blot (Fig. 8b, Additional file 9: Figure S9a) and qRT-PCR (Fig. 8c, Additional file 9: Figure S9b) in GC cells. This result illustrates that both I1QB and

I3QB are indispensable for the production of circNRIP1. In the next step, we attempted to determine whether QKI could regulate circNRIP1 formation post-transcriptionally during GC development. We knocked down QKI and observed a significant reduction in circNRIP1 but not pre-mNRIP1 or mNRIP1 (Fig. 8d, Additional file 9: Figure S9c). In addition, we performed an RNA immunoprecipitation (RIP) experiment to observe whether QKI could bind I1QB or I3QB. Subsequently, the enrichment of I1QB and I3QB was observed when we used an antibody against QKI (Fig. 8e, Additional file 9: Figure S9d). In the next step, we detected higher QKI expression levels in GC tumour tissues relative to adjacent normal stomach tissues among 40 patients by immunohistochemistry (Fig. 8f). We also performed qRT-PCR on these 40 patients and discovered that the expression level of circNRIP1 was positively correlated with the QKI histochemistry score (Fig. 8g).

In summary, the upregulation of circNRIP1 was attributed at least in part to the promotion of QKI in GC tissues.

CircNRIP1 plays a tumour promotor role in GC growth in vivo

Patient-derived xenograft (PDX) mouse models were further used to assess the effects of circNRIP1 on GC growth in vivo. The circNRIP1 overexpression plasmid and cholesterol-conjugated circNRIP1 siRNA were continuously injected intratumorally into PDX mice (Fig. 9a). First, the donor patients were clinically characterized (Additional file 9: Figure S9e), and the engrafted tumours were histopathologically analysed (Additional file 9: Figure S9f). The expression level of circNRIP1 was higher, and the level of miR-149-5p was lower in these 3 GC clinical specimens relative to the adjacent normal tissues (Additional file 9: Figure S9f). Additionally, we found that circNRIP knockdown in vivo significantly blocked tumour growth in terms of tumour weight and volume relative to the negative control group, whereas the overexpression of circNRIP1 promoted the growth of xenografted tumours (Fig. 9b, Additional file 9: Figure S9g). Furthermore, qRT-PCR was performed in PDX tumours, and we found increased and persistent levels of

circNRIP1 in the circNRIP1 overexpression plasmid-treated groups relative to the NC group and lower levels of circNRIP1 in long-term circNRIP1 siRNA-treated groups (Fig. 9c). The expression levels of p-AKT1, p-mTOR, PFK and LC3 were observed in PDX tumours (Fig. 9d). Moreover, AKT1 and mTOR expression levels were also determined by immunohistochemistry (Fig. 9e). The aforementioned results suggested that circNRIP1 promoted energy production activities, such as the Warburg effect, and inhibited catabolic activities, such as autophagy, by activating the AKT1/mTOR signalling pathway to ultimately favour GC tumour growth in vivo. Considering that circNRIP1 could successfully upregulate EMT markers in GC cells and be transmitted by exosomes to promote GC metastasis via EMT, we again verified the positive interaction between circNRIP1 and EMT in the aforementioned PDX tumour tissues (Fig. 9f).

Collectively, intratumoral knockdown of circNRIP1 effectively reduced PDX tumour growth in BALB/c nude mice via downstream metabolism alterations mediated by the AKT/mTOR signalling pathway.

Discussion

In our study, we performed next-generation sequencing to detect differentially expressed circRNAs within GC tissues relative to adjacent normal stomach tissues. We selected circNRIP1, an upregulated circRNA with a high fold-change and significant *P* value in tumour tissues, to investigate its regulatory role in GC progression. First, we applied bioinformatic prediction and RNA immunoprecipitation to verify whether miR-149-5p is the binding miRNA of circNRIP1. Subsequently, we utilized a dual-luciferase assay to verify their complementary binding. Many researchers have reported the regulatory role of miR-149-5p on AKT1 in other cancers [48, 49]. In the next phase, the expression levels of circNRIP1 and AKT1, which is a ceRNA of circNRIP1, were both verified by polymerase chain reaction (qRT-PCR) in GC tissues and GC cell lines. Moreover, the AKT/mTOR axis is a classic signalling pathway that sustains energy homeostasis through energy production activities, such as the Warburg effect to satisfy the proliferation needs of GC cells [50, 51]. Additionally, AKT/mTOR enables anabolic metabolism, such as protein synthesis, and blocks catabolic activities, such as autophagy, to ultimately favour cell growth in GC [52]. Additionally, the AKT/mTOR axis exerts a positive role on EMT, which promotes tumour metastasis [53, 54]. Thus, we sought to determine the interactions between the aforementioned metabolic activities and circNRIP1.

According to our experiments and analysis, circNRIP1 knockdown successfully blocked the proliferation, migration, invasion and AKT1 expression levels of GC cells.

MiR-149-5p inhibition phenocopied circNRIP1 overexpression in GC cells, and miR-149-5p overexpression blocked the malignant behaviours of circNRIP1. Moreover, we proved that circNRIP1 could be transmitted by exosomal communication between GC cells, and exosomal circNRIP1 could further promote tumour metastasis in vivo. We also demonstrated that the RNA binding protein QKI could promote the circular transcription of the NRIP1 gene. In the final step, the tumour promoter role of circNRIP1 was verified in PDX models.

Although the mechanisms explaining how circRNA acts as a regulator during carcinogenesis and cancer progression have not been fully elucidated, many researchers have stated that circRNAs can function as ceRNAs in tumour biology [55, 56]. The ceRNA hypothesis is derived from many evidence-based reports and illustrates interactions between non-coding RNAs and coding RNAs via miRNA mediation, as well as how non-coding RNAs compete with each other to absorb miRNA and finally affect tumour development at the posttranscriptional level. The biogenesis of circRNAs is now generally believed to occur via non-linear reverse splicing [57]. CircRNAs are stable relative to miRNAs because their 5' cap and 3' tail are buried in the loop [14]. Many researchers have reported that circRNAs act as miRNA sponges to modulate the expression of tumour suppressor or promoter genes through the circRNA-miRNA-mRNA axis [58]. In our study, we showed that circNRIP1 acts as a sponge absorbing miR-149-5p to modulate AKT1 expression in GC.

With the development of our knowledge of circRNAs, many researchers have recognized that circRNAs do not only act as miRNA sponges, and some circRNAs can sponge trans-acting elements to promote or block the transcription of parental genes. Moreover, certain exonic-intronic circRNAs (EIciRNAs) gather in the nucleus and bind to the linear transcripts of their parental genes to mediate mRNA translation. Additionally, some circRNAs are even translated into proteins to fulfil crucial biological functions, whereas several circRNAs are wrapped into exosomes to promote tumour metastasis.

Conclusions

We demonstrated that circNRIP1 is significantly upregulated in human gastric cancer tissues and can successfully sponge miR-149-5p to promote the proliferation, migration and invasion of GC cells. We also found that inhibition of circNRIP1 can block the malignant behaviour of GC cells through the AKT1/mTOR signalling pathway. We proved that circNRIP1 assumes the role of a miRNA sponge and that circNRIP1 inhibition will be a promising therapeutic target in GC in the years to come.

Additional files

Additional file 1: Figure S1. (A). We verified the significantly upregulated pull-down efficiency of the circNRIP1 probe in MKN-45 and BGC-823 cells transfected with the circNRIP1 overexpression plasmid (pcDNA3.1). (B). We observed that miR-149-5p silencing promoted the cell proliferation rate as indicated by the CCK8 assay, and overexpression of miR-149-5p exerted the opposite effect on the GC cell proliferation rate. (C). We observed that miR-149-5p silencing significantly promoted DNA synthesis as determined by the Edu assay, and overexpression of miR-149-5p exerted the opposite effect on GC cell DNA synthesis, scale bar = 100 μ m. (D). The knockdown of miR-149-5p successfully promoted the migration and invasion ability of GC cells, and overexpression of miR-149-5p exerted the opposite effect on metastasis, scale bar = 200 μ m. All data are presented as the mean \pm SEM. * p < 0.05, ** p < 0.01, *** p < 0.001. (TIF 2828 kb)

Additional file 2: Figure S2. (A). We used qRT-PCR to verify the circNRIP1 silencing efficiency and rule out the possibility that circNRIP1 siRNA might exert effects on the mRNA level of NRIP1 (linear NRIP1). (B). We detected lower expression levels of AKT1 by qRT-PCR after knocking down circNRIP1 in MKN-45 and BGC-823 GC cells. (C). The knockdown of circNRIP1 successfully reduced the migration ability of GC cells, and overexpression of circNRIP1 exerted the opposite effect on migration as indicated by the wound healing assay, scale bar = 100 μ m. (D). The sequences and transfection efficiencies of miR-149-5p mimics and inhibitors were confirmed by qRT-PCR. All data are presented as the mean \pm SEM. * p < 0.05, ** p < 0.01, *** p < 0.001. (TIF 1463 kb)

Additional file 3: Figure S3. (A). We performed a series of glycolysis detection experiments. We found that knockdown of circNRIP1 reduced lactate contents, glucose uptake and ATP production in MKN-45 and BGC-823 cells. However, the reduction in glycolysis activity was restored when we knocked down both circNRIP1 and miR-149-5p. (D). The extracellular acidification rate (ECAR) was measured. Knockdown of both miR-149-5p and circNRIP1 rescued the reduced glycolysis rate and glycolytic capacity observed when knocking down only circNRIP1. All data are presented as the mean \pm SEM. * p < 0.05, ** p < 0.01, *** p < 0.001. (TIF 350 kb)

Additional file 4: Figure S4. (A). A cluster heat map was used to show the expression variations of these circRNA transcripts in cancerous tissues relative to matched normal tissues. All data are presented as the mean \pm SEM. * p < 0.05, ** p < 0.01, *** p < 0.001. (TIF 1364 kb)

Additional file 5: Figure S5. (A). Potential binding between circNRIP1 and miR-149-5p based on their complementary sequences. (B). We confirmed that the low level of miR-149-5p was positively correlated with the OS (median survival of 58 months vs 21 months; P = 0.0007, log-rank test) and DFS (median survival of 56 months vs 19 months; P = 0.0002, log-rank test) of GC patients. (C). We found that AKT1 was significantly upregulated in GC tissues (415 GC tissues vs 34 normal tissues), and patients with high levels of AKT1 (298 GC tissues vs 94 normal tissues) had lower OS based on an analysis of the TCGA database. All data are presented as the mean \pm SEM. * p < 0.05, ** p < 0.01, *** p < 0.001. (TIF 2223 kb)

Additional file 6: Figure S6. (A). We observed that circNRIP1 silencing significantly inhibited colony formation ability, and overexpression of circNRIP1 exerted the opposite effect on colony formation in BGC-823 cells. (B). We observed that circNRIP1 silencing significantly inhibited the cell proliferation rate, as indicated by the CCK8 assay, and overexpression of circNRIP1 exerted the opposite effect on the GC cell proliferation rate in BGC-823 cells. (C). We observed that circNRIP1 silencing significantly inhibited DNA synthesis, as determined by the Edu assay, and overexpression of circNRIP1 exerted the opposite effect on GC cell DNA synthesis as indicated by the Edu assay in BGC-823 cells, scale bar = 100 μ m. (D). Knockdown of circNRIP1 successfully reduced the migration and invasion ability of GC cells, and overexpression of circNRIP1 exerted the opposite effect on metastasis, as indicated by the transwell assay in BGC-823 cells, scale bar = 200 μ m. (E). We observed that both circNRIP1 knockdown and miR-149-5p overexpression significantly inhibited the growth of the organoid models, while circNRIP1 overexpression

promoted organoid model survival. All data are presented as the mean \pm SEM. * p < 0.05, ** p < 0.01, *** p < 0.001. (TIF 4931 kb)

Additional file 7: Figure S7. (A). Knockdown of circNRIP1 and miR-149-5p significantly reversed the expression levels of AKT1/mTOR pathway molecules, certain metabolism markers and EMT markers achieved by knocking down only circNRIP1 in BGC-823 cells. (B). We observed that the reduction of GC cell proliferation mediated by circNRIP1 knockdown was successfully blocked by miR-149-5p inhibition in BGC-823 cells, scale bar = 100 μ m. (C). We observed that the reduction of metastasis of GC cells mediated by circNRIP1 knockdown was successfully blocked by miR-149-5p inhibition in BGC-823 cells, scale bar = 100 μ m. All data are presented as the mean \pm SEM. * p < 0.05, ** p < 0.01, *** p < 0.001. (TIF 3849 kb)

Additional file 8: Figure S8. (A). We used a transmission electron microscope (TEM) to determine the existence and morphology of exosomes purified from GC cell medium (exosome-free FBS) in the BGC-823 cells, scale bar = 25 μ m. (B). Red exosome signals were found in the cytoplasm of GFP-labelled tumour cells when exo-RFP GC cells were mixed with the same amount of GFP-labelled GC cells for 72 hours in the BGC-823 cells, scale bar = 50 μ m. (C). We then purified exosomes and added them into GFP-labelled MKN-45 or BGC-823 GC cells. The red signal of circNRIP1 similarly appeared in the cytoplasm of GFP-labelled GC cells after 72 hours in the BGC-823 cells, scale bar = 50 μ m. (D). We performed qRT-PCR and detected higher circNRIP1 expression in exosomes purified from circNRIP1-overexpressing GC cells relative to those from NC cells in the BGC-823 cells. (E). We detected upregulated AKT1, mTOR and EMT markers in GC cells by co-culturing them with exosomes of OV circNRIP1 GC cells (OV exosomes) for 72 h via western blot in the BGC-823 cells. (F). According to the luciferase intensities detected in the thoracic cavity, we found that GC cells treated with OV exosomes showed higher metastasis potential in the BGC-823 cells. (G). We harvested lung tissues for H&E staining to characterize the cancerous nodes. Cancerous node size was consistent with luciferase intensity, scale bar = 200 μ m. All data are presented as the mean \pm SEM. * p < 0.05, ** p < 0.01, *** p < 0.001. (TIF 7218 kb)

Additional file 9: Figure S9. (A). We observed that only the wild-type plasmid (#4), and neither the I1QB nor I3QB deletion constructs (#1-3), could overexpress circNRIP1 according to northern blotting in BGC-823 cells. (B). We observed that only the wild-type plasmid (#4), and neither the I1QB nor I3QB deletion constructs (#1-3), could overexpress circNRIP1 according to qRT-PCR in BGC-823 cells. (C). We knocked down QKI and observed a significant reduction in circNRIP1 but not pre-mNRIP1 or mNRIP1 in BGC-823 cells. (D). Enrichment of I1QB and I3QB was observed when we used an antibody against QKI in BGC-823 cells. (E). The donor patients were clinically characterized. (F). The engrafted tumours were histopathologically analysed, scale bar = 100 μ m. (G). We found that circNRIP1 knockdown in vivo significantly blocked tumour growth in terms of tumour weight and volume relative to the negative control group, whereas overexpression of circNRIP1 promoted the growth of xenografted tumours. All data are presented as the mean \pm SEM. * p < 0.05, ** p < 0.01, *** p < 0.001. (TIF 6448 kb)

Abbreviations

3'-UTR: 3'-Untranslated region; DFS: Disease-free survival; EMT: Epithelial-mesenchymal transition; GC: Gastric cancer; I1QB: Intron 1 QKI binding sequences; I3QB: Intron 3 QKI binding sequences; mTOR: Mammalian target of rapamycin; OS: Overall survival; PDX: Patient-derived xenograft; QKI: Quaking; qRT-PCR: Quantitative real-time PCR; siRNA: Short interfering RNA

Acknowledgements

Not applicable.

Funding

This work was partially supported by the National Natural Science Foundation of China (81572362); the National Natural Science Foundation Project of International Cooperation (NSFC-NIH, 81361120398); the Primary Research & Development Plan of Jiangsu Province (BE2016786); the Program for Development of Innovative Research Team in the First Affiliated Hospital of NJMU; the Priority Academic Program Development of Jiangsu Higher

Education Institutions (PAPD, JX10231801); the 333 Project of Jiangsu Province (BRA2015474); Jiangsu Key Medical Discipline (General Surgery) (ZDXKA2016005); and the Jiangsu Key Lab of Cancer Biomarkers, Prevention and Treatment, Collaborative Innovation Center for Cancer Personalized Medicine, Nanjing Medical University.

Availability of data and materials

The datasets used and/or analysed during the current study are available from the corresponding author upon reasonable request.

Authors' contributions

SW and HW participated in the experimental design and data analysis. JC performed some of the experiments. XZ conceived of the project, performed most of the experiments and was a major contributor in writing the manuscript. All of the authors read and approved the final manuscript.

Ethics approval and consent to participate

We obtained human GC tissues and adjacent normal tissues from GC patients at the First Affiliated Hospital of Nanjing Medical University. The ethics committee of Nanjing Medical University approved all of our experiments. BALB/c-null mice and SCID mice were purchased from the animal centre of Nanjing Medical University (Nanjing, China) and bred under special pathogen-free (SPF) conditions. We followed protocols approved by the Institutional Committee on Animal Care of Nanjing Medical University.

Consent for publication

Not applicable.

Competing interests

The authors declare that they have no competing interests.

Publisher's Note

Springer Nature remains neutral with regard to jurisdictional claims in published maps and institutional affiliations.

Author details

¹Department of General Surgery, The First Affiliated Hospital of Nanjing Medical University, No.300, Guangzhou Road, Nanjing, Jiangsu Province, China. ²Department of Surgical Oncology, University of Miami, Miami, USA. ³Collaborative Innovation Center For Cancer Personalized Medicine, Nanjing Medical University, Nanjing 210029, Jiangsu Province, China. ⁴Department of General Surgery, The Affiliated Huaian No.1 People's Hospital of Nanjing Medical University, Huaian 223300, Jiangsu, China.

Received: 16 October 2018 Accepted: 27 December 2018

Published online: 04 February 2019

References

1. Torre LA, et al. Global cancer statistics, 2012. *CA Cancer J Clin*. 2015;65(2): 87–108.
2. Hamashima C. Current issues and future perspectives of gastric cancer screening. *World J Gastroenterol*. 2014;20(38):13767–74.
3. Shin VY, Chu KM. MiRNA as potential biomarkers and therapeutic targets for gastric cancer. *World J Gastroenterol*. 2014;20(30):10432–9.
4. Allemani C, Weir HK, Carreira H, Harewood R, Spika D, Wang XS, et al. Global surveillance of cancer survival 1995e2009: analysis of individual data for 25,676,887 patients from 279 population-based registries in 67 countries (CONCORD-2). *Lancet*. 2015;385(9972):977–101.
5. Wang QX, et al. Altered MiRNA expression in gastric cancer: a systematic review and meta-analysis. *Cell Physiol Biochem*. 2015;35(3):933–44.
6. Huang YK, Yu JC. Circulating microRNAs and long non-coding RNAs in gastric cancer diagnosis: an update and review. *World J Gastroenterol*. 2015; 21(34):9863–86.
7. Virgilio E, et al. Long non-coding RNAs in the gastric juice of gastric cancer patients. *Pathol Res Pract*. 2018;214(9):1239–46.
8. Soslau G. Circular RNA (circRNA) was an important bridge in the switch from the RNA world to the DNA world. *J Theor Biol*. 2018;447:32–40.
9. Dong R, et al. Increased complexity of circRNA expression during species evolution. *RNA Biol*. 2017;14(8):1064–74.
10. Ashwal-Fluss R, et al. circRNA biogenesis competes with pre-mRNA splicing. *Mol Cell*. 2014;56(1):55–66.
11. Thomson DW, Dinger ME. Endogenous microRNA sponges: evidence and controversy. *Nat Rev Genet*. 2016;17(5):272–83.
12. Zhang Y, Zhang XO, Chen T, Xiang JF, Yin QF, Xing YH, et al. Circular intronic long noncoding RNAs. *Mol Cell*. 2013;51:792–806.
13. Li Z, Huang C, Bao C, Chen L, Lin M, Wang X, et al. Exon-intron circular RNAs regulate transcription in the nucleus. *Nat Struct Mol Biol*. 2015;22:256–64.
14. Jeck WR, Sharpless NE. Detecting and characterizing circular RNAs. *Nat Biotechnol*. 2014;32:453–461.
15. Qu S, Zhong Y, Shang R, Zhang X, Song W, Kjems J, et al. The emerging landscape of circular RNA in life processes. *RNA Biol*. 2016;11:1–8.
16. Qu S, Yang X, Li X, Wang J, Gao Y, Shang R, Sun W, Dou K, Li H. Circular RNA: a new star of noncoding RNAs. *Cancer Lett*. 2015;365(2):141–8.
17. Yang Y, et al. Extensive translation of circular RNAs driven by N(6)-methyladenosine. *Cell Res*. 2017;27(5):626–41.
18. Legnini I, et al. Circ-ZNF609 is a circular RNA that can be translated and functions in Myogenesis. *Mol Cell*. 2017;66(1):22–37.e9.
19. Hansen TB, et al. Natural RNA circles function as efficient microRNA sponges. *Nature*. 2013;495(7441):384–8.
20. Liu W, et al. Circular RNA hsa_circRNA_103809 promotes lung cancer progression via facilitating ZNF121-dependent MYC expression by sequestering miR-4302. *Biochem Biophys Res Commun*. 2018;500(4):846–51.
21. He JH, et al. The CircRNA-ACAP2/Hsa-miR-21-5p/ Tiam1 regulatory feedback circuit affects the proliferation, migration, and invasion of colon cancer SW480 cells. *Cell Physiol Biochem*. 2018;49(4):1539–50.
22. Dong Y, He D, Peng Z, Peng W, Shi W, Wang J, et al. Circular RNAs in cancer: an emerging key player. *J Hematol Oncol*. 2017;10:2.
23. Zhong Y, Du Y, Yang X, Mo Y, Fan C, Xiong F, Ren D, Ye X, Li C, Wang Y, Wei F, Guo C, Wu X, Li X, Li Y, Li G, Zeng Z, Xiong W. Circular RNAs function as ceRNAs to regulate and control human cancer progression. *Mol Canc*. 2018;17:79.
24. Chen Y, et al. Circular RNA circAGO2 drives cancer progression through facilitating HuR-repressed functions of AGO2-miRNA complexes. *Cell Death Differ*. 2018. [Epub ahead of print].
25. Li Y, et al. CircHIPK3 sponges miR-558 to suppress heparanase expression in bladder cancer cells. *EMBO Rep*. 2017;18(9):1646–59.
26. Han D, Li J, Wang H, Su X, Hou J, Gu Y, et al. Circular RNA circMTO1 acts as the sponge of microRNA-9 to suppress hepatocellular carcinoma progression. *Hepatology*. 2017;66:1151–64.
27. Xia P, Xu XY. PI3K/Akt/mTOR signaling pathway in cancer stem cells: from basic research to clinical application. *Am J Cancer Res*. 2015;5(5):1602–9.
28. Su MA, et al. An invertebrate Warburg effect: a shrimp virus achieves successful replication by altering the host metabolome via the PI3K-Akt-mTOR pathway. *PLoS Pathog*. 2014;10(6):e1004196.
29. Lu CL, et al. Tumor cells switch to mitochondrial oxidative phosphorylation under radiation via mTOR-mediated hexokinase II inhibition—a Warburg-reversing effect. *PLoS One*. 2015;10(3):e0121046.
30. Polivka JJ, Janku F. Molecular targets for cancer therapy in the PI3K/AKT/mTOR pathway. *Pharmacol Ther*. 2014;142(2):164–75.
31. Steinbichler TB, et al. The role of exosomes in cancer metastasis. *Semin Cancer Biol*. 2017;44:170–81.
32. Wang X, et al. Investigation of the roles of exosomes in colorectal cancer liver metastasis. *Oncol Rep*. 2015;33(5):2445–53.
33. Qin W, et al. Exosomes in human breast Milk promote EMT. *Clin Cancer Res*. 2016;22(17):4517–24.
34. Kim J, et al. Exosome cargo reflects TGF-beta1-mediated epithelial-to-mesenchymal transition (EMT) status in A549 human lung adenocarcinoma cells. *Biochem Biophys Res Commun*. 2016;478(2):643–8.
35. Mahe MM, et al. Establishment of gastrointestinal epithelial organoids. *Curr Protoc Mouse Biol*. 2013;3(4):217–40.
36. Jin L, et al. Tumor suppressor miR-149-5p is associated with cellular migration, proliferation and apoptosis in renal cell carcinoma. *Mol Med Rep*. 2016;13(6):5386–92.
37. Okato A, et al. Dual strands of pre-miR-149 inhibit cancer cell migration and invasion through targeting FOXM1 in renal cell carcinoma. *Int J Mol Sci*. 2017;18(9):1969.
38. Zhang Y, et al. Comprehensive analysis of microRNA-regulated protein interaction network reveals the tumor suppressive role of microRNA-149 in human hepatocellular carcinoma via targeting AKT-mTOR pathway. *Mol Cancer*. 2014;13:253.
39. Ghasemi A, Fallah S, Ansari M. MicroRNA-149 is epigenetically silenced tumor-suppressive microRNA, involved in cell proliferation and

- downregulation of AKT1 and cyclin D1 in human glioblastoma multiforme. *Biochem Cell Biol.* 2016;94(6):569–76.
40. Zhang G, et al. EphB3-targeted regulation of miR-149 in the migration and invasion of human colonic carcinoma HCT116 and SW620 cells. *Cancer Sci.* 2017;108(3):408–18.
 41. Chang L, Li K, Guo T. miR-26a-5p suppresses tumor metastasis by regulating EMT and is associated with prognosis in HCC. *Clin Transl Oncol.* 2017;19(6): 695–703.
 42. Yeung KT, Yang J. Epithelial-mesenchymal transition in tumor metastasis. *Mol Oncol.* 2017;11(1):28–39.
 43. Larue L, Bellacosa A. Epithelial-mesenchymal transition in development and cancer: role of phosphatidylinositol 3' kinase/AKT pathways. *Oncogene.* 2005;24(50):7443–54.
 44. Rafael, D., et al. EMT blockage strategies: targeting Akt dependent mechanisms for breast cancer metastatic behaviour modulation. *Curr Gene Ther.* 2015;15(3):300–312.
 45. Li X, Yang L, Chen LL. The biogenesis, functions, and challenges of circular RNAs. *Mol Cell.* 2018;71(3):428–42.
 46. Ebbesen KK, Kjems J, Hansen TB. Circular RNAs: identification, biogenesis and function. *Biochim Biophys Acta.* 2016;1859(1):163–8.
 47. Conn SJ, et al. The RNA binding protein quaking regulates formation of circRNAs. *Cell.* 2015;160(6):1125–34.
 48. Xu RD, et al. miR-149-5p inhibits cell growth by regulating TWEAK/Fn14/PI3K/AKT pathway and predicts favorable survival in human osteosarcoma. *Int J Immunopathol Pharmacol.* 2018;32:2058738418786656. https://journals.sagepub.com/doi/full/10.1177/2058738418786656?url_ver=Z39.88-2003&rft_id=ori%3Arid%3Acrossref.org&rft_dat=cr_pub%3Dpubmed#articleCitationDownloadContainer.
 49. Wu J, et al. Pre-miR-149 rs71428439 polymorphism is associated with increased cancer risk and AKT1/cyclinD1 signaling in hepatocellular carcinoma. *Int J Clin Exp Med.* 2015;8(8):13628–33.
 50. Mosca E, et al. Systems biology of the metabolic network regulated by the Akt pathway. *Biotechnol Adv.* 2012;30(1):131–41.
 51. Giguere V. Canonical signaling and nuclear activity of mTOR-a teamwork effort to regulate metabolism and cell growth. *FEBS J.* 2018;285(9):1572–88.
 52. Heras-Sandoval D, et al. The role of PI3K/AKT/mTOR pathway in the modulation of autophagy and the clearance of protein aggregates in neurodegeneration. *Cell Signal.* 2014;26(12):2694–701.
 53. Yang Y, et al. DEK promoted EMT and angiogenesis through regulating PI3K/AKT/mTOR pathway in triple-negative breast cancer. *Oncotarget.* 2017; 8(58):98708–22.
 54. Wu ZH, et al. MiR-616-3p promotes angiogenesis and EMT in gastric cancer via the PTEN/AKT/mTOR pathway. *Biochem Biophys Res Commun.* 2018; 501(4):1068–73.
 55. Qi X, et al. ceRNA in cancer: possible functions and clinical implications. *J Med Genet.* 2015;52(10):710–8.
 56. Ergun S, Oncocers OS. ceRNA-mediated cross-talk by sponging miRNAs in oncogenic pathways. *Tumour Biol.* 2015;36(5):3129–36.
 57. Chen, L.L. The biogenesis and emerging roles of circular RNAs. *Nat Rev Mol Cell Biol.* 2016;17:205–211.
 58. Xie F, et al. Circular RNA BCRC-3 suppresses bladder cancer proliferation through miR-182-5p/p27 axis. *Mol Cancer.* 2018;17(1):144.

Ready to submit your research? Choose BMC and benefit from:

- fast, convenient online submission
- thorough peer review by experienced researchers in your field
- rapid publication on acceptance
- support for research data, including large and complex data types
- gold Open Access which fosters wider collaboration and increased citations
- maximum visibility for your research: over 100M website views per year

At BMC, research is always in progress.

Learn more biomedcentral.com/submissions

